8-19-2024

Deconvolving Provenance Signatures of Pliocene-Pleistocene Coastal Loess Deposits Along the Atlantic Margin of Argentina

Will Robert Quanrud
University of South Carolina

DECONVOLVING PROVENANCE SIGNATURES OF PLIOCENE-PLEISTOCENE COASTAL LOESS DEPOSITS ALONG THE ATLANTIC MARGIN OF ARGENTINA

by

Will Robert Quanrud

Bachelor of Science
Ohio University, 2021

Submitted in Partial Fulfillment of the Requirements

For the Degree of Master of Science in

Geological Sciences

College of Arts and Sciences

University of South Carolina

2024

Accepted by:

Andrew Leier, Director of Thesis

David Barbeau, Reader

Alexander Pullen, Reader

Ann Vail, Dean of the Graduate School

ACKNOWLEDGEMENTS

This research was funded by the U.S. National Science Foundation (EAR-1910510). We thank the Arizona LaserChron Center at the University of Arizona, USA.

ABSTRACT

Dust derived from southern South America provides critical nutrients for autotrophic organisms in the South Atlantic Ocean and the Southern Ocean, such that dust may ultimately affect the concentration of atmospheric CO_2. Expansive sand and loess deposits are exposed in Central Argentina, recording millions of years of eolian activity; however, the provenance and transport pathways of this dust remain unclear. Loess deposits ranging in age from Pliocene to upper Pleistocene are present along the Atlantic margin of Argentina and provide information on sediment transport pathways for the last 4 million years. Nine samples of loess were collected and analyzed using detrital zircon U-Pb geochronology to better understand the source of these coastal loess deposits. All nine samples have similar provenance with most samples containing an age population from 0–30 Ma, 60–120 Ma, 160–200 Ma, 240–290 Ma, 350–400 Ma, 440–480 Ma, 520–640, and 960–1200 Ma. The age populations present in the coastal loess deposits are indistinguishable from detrital zircon age populations in late Miocene eolian and fluvial deposits from central Argentina, as well as late Pleistocene–Holocene eolian and fluvial deposits in the Pampas of central Argentina. This correlation indicates the coastal loess deposits are part of the same longstanding eolian system that deposited eolian sand and loess in central Argentina. While these deposits are part of the same eolian system with the same source as the Pampas, a vertical trend is present throughout the coastal loess deposits suggesting that minor changes in sediment source may have occurred over time. The data indicate an increased influx of sediment from northern

Patagonia relative to other portions of the Andes. The cause of this trend remains unclear; however, dynamic climatic conditions during the Pleistocene may have been a primary driver of this provenance shift. Several hypotheses can explain how the coastal loess deposits received relatively greater influxes from more southerly locations. Overall, the coastal loess deposits represent an important record of eolian deposits from an eolian system that has been active in central Argentina for the last 7 million years.

TABLE OF CONTENTS

LIST OF FIGURES

CHAPTER 1

INTRODUCTION

. Wind-blown dust from southern South America plays an important role in regional and global systems. This dust lands in the South Atlantic Ocean, providing critical nutrients that facilitate primary productivity (Martin et al., 1988; Abelman et al., 2006). During periods of relatively greater dust flux, this process is hypothesized to reduce atmospheric CO_2 (Martin, 1990; Martin et al., 1990; Cassar et al., 2007; Martínez-Garcia et al., 2011; Mahowald et al., 2017). Whereas the impact of dust on the Southern Ocean has been investigated for decades (e.g., Martin et al., 1990) there are few constraints on the sediment sources, transport pathways and depositional histories of eolian material in the source area of southern South America. Furthermore, studies that have been reported have limited differentiation between proto-sources and primary sources of sediment in Argentina. Previous studies helped establish general sediment provenance (Teruggi, 1957; González Bonorino 1966; Zárate and Blasi, 1993; Iriondo, 1997), but were limited by non-unique sediment sources and the analytical techniques available at the time. As a result, the dust production portion of this critical system remains poorly constrained.

The history of eolian transport in southern South America is arguably best preserved within upper Cenozoic deposits in the Pampas of central Argentina, which are covered by extensive (300,000 km^2) upper Pleistocene-Holocene eolian sand deposits

referred to as the Pampean Sand Sea (Figure 1.1; Teruggi, 1957; Iriondo, 1990; Imbellone and Teruggi, 1993; Zárate and Blasi, 1993; Iriondo, 1997; Kröhling, 1999; Zárate and Tripaldi, 2012; Tripaldi et al., 2013; Bruner et al., 2022; Garzanti et al., 2022). The Pampean Sand Sea is bounded on the east and north by upper Pleistocene–Holocene loess and loessoid (reworked loess) deposits, which when combined with the Sand Sea covers an area of >400,000 km2 (Figure 1.1). The sediments comprising these deposits are derived from the Andes, including exhumed rocks within the Cordillera and volcanic detritus from the Andean arc (Teruggi 1957; Folguera & Zarate 2011, Tripaldi et al., 2018, Capaldi et al., 2021; Garzanti et al., 2021a; Garzanti et al., 2022). Detritus from the Andes is transported to the foreland by fluvial systems, where they were entrained and transported by prevailing winds (Brunner et al., 2022; Garzanti et al., 2022). Underlying the upper Pleistocene-Holocene units are even older deposits of Late Miocene age that indicate the regional eolian system has been active for millions of years. Detrital zircon data from these older strata are nearly identical to those in the overlying upper Pleistocene-Holocene deposits, indicating the sediment sources and transport pathways responsible for the Pampean Sand Sea and surrounding loess belt were established and operating as far back as the Late Miocene (ca. 6-8 Ma; Stubbins et al., 2023).

Between the upper Miocene and upper Pleistocene–Holocene eolian deposits in the Pampas is a regional unconformity. Across central Argentina, eolian sediments of Pliocene–early Pleistocene age are absent, except in a very limited area of the eastern coast of central Argentina (Teruggi, 1957; Zárate and Fasano, 1989; Zárate and Blasi, 1993). Here, Pliocene–Pleistocene loess and loessoid units are exposed along the Atlantic coast for >30 km. These units have been divided into several formations based on

detailed stratigraphic studies (e.g., Zárate and Fasano, 1989) and their depositional ages have been constrained with paleomagnetic chronostratigraphy and South American land mammal ages (Zárate and Fasano, 1989; Orgeira, 1990; Cione and Tonni, 1995; Bidegain and Rico, 2012; Prevosti et al., 2021). Because of the limited geographic extent of these exposures, and the absence of deposits of this age in the Pampas, these loess units raise several important questions for the late Cenozoic eolian history of central Argentina. There is uncertainty as to how these coastal loess deposits are related to the eolian deposits in the Pampas. Do the coastal loess deposits share the same sediment source as the Pampean eolian deposits of Miocene and late Pleistocene-Holocene age? Furthermore, what can these coastal deposits tell us about the evolution of eolian activity in central Argentina during the Pliocene-Pleistocene?

To better understand the provenance of Pliocene-Pleistocene loess deposits along the Atlantic margin of central Argentina and evaluate how these units compare to Miocene and upper Pleistocene-Holocene deposits, we collected N= 9 samples from middle Pliocene to Pleistocene loess units exposed along the Argentine Atlantic margin for detrital zircon U-Pb geochronology. In total, we obtained n= 3941 new U-Pb detrital zircon ages from these analyses, with an average of n= >400 new U-Pb zircon ages per sample. These new data indicate the Pliocene-Pleistocene loess deposited along the Argentine coast was derived from the same sediment sources as the Miocene and upper Pleistocene/Holocene loess deposits in the Pampas of Argentina (Bruner et al., 2022; Stubbins et al., 2023). There are also vertical changes in the relative proportion of detrital zircon age populations within the coastal loess deposits. Unmixing models suggest these

changes are reflecting changing contributions from specific sediment sources in the Andes throughout deposition.

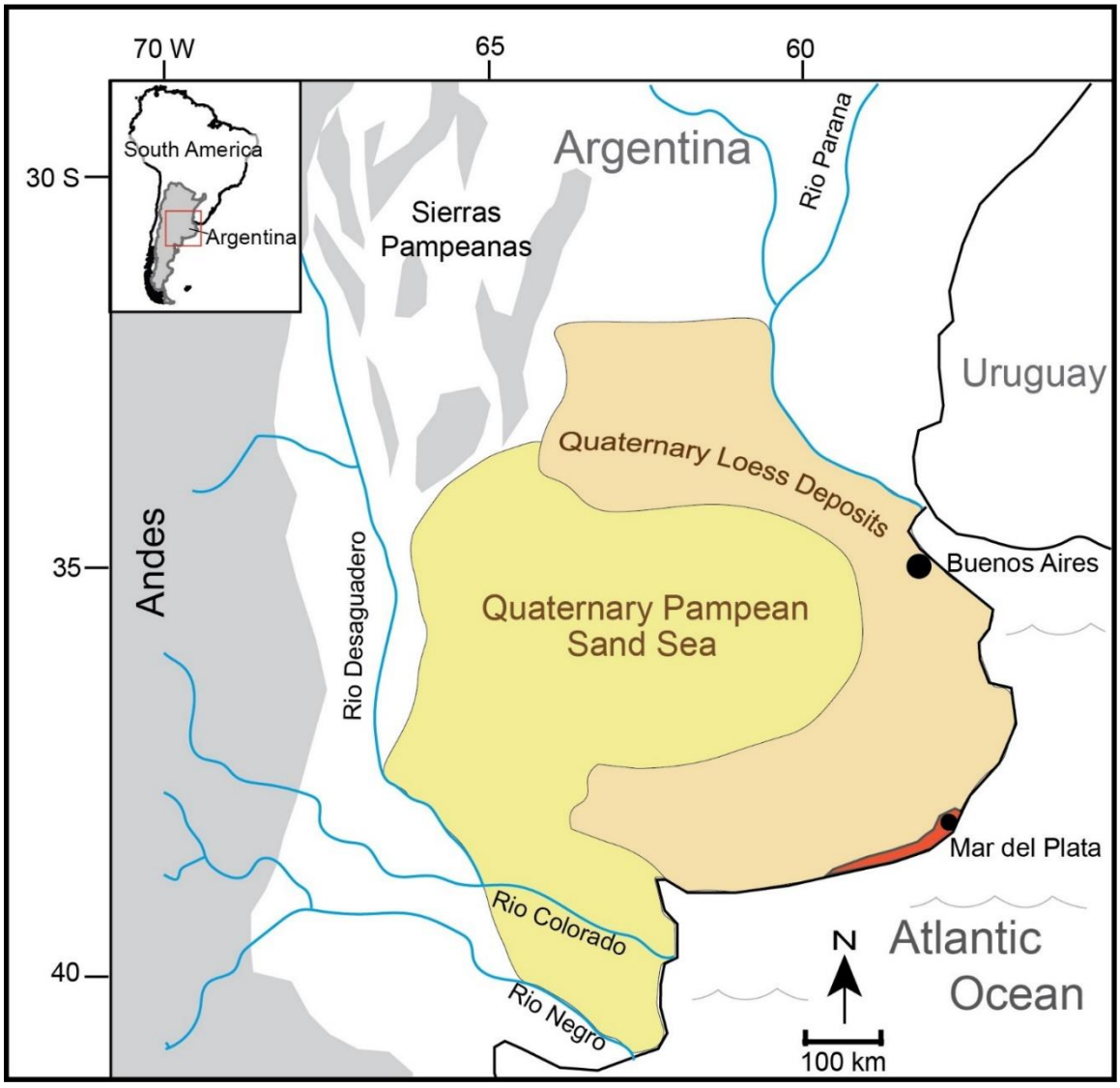

Figure 1.1: Diagram of Central Argentina outlining the location of Pleistocene-Holocene eolian deposits including the Pampean Sand Sea (yellow) and Loess Belt (brown) (Teruggi, 1957; Iriondo, 1990; Imbellone and Teruggi, 1993; Zárate and Blasi, 1993; Iriondo, 1997; Kröhling, 1999; Zárate and Tripaldi, 2012; Bruner et al., 2022; Garzanti et al., 2022). Major rivers are shown with blue lines and two cities (Buenos Aires and Mar del Plata) are labeled for reference. The red near Mar del Plata represents the Pliocene-Pleistocene coastal loess deposits exposed along the coast of Argentina.

CHAPTER 2

POVENANCE AND TRANSPORT OF PLIOCENE-PLEISTOCENE LOESS TO BETTER ESTABLISH THE GEOLOGIC HISTORY OF THE PAMPEAN EOLIAN SYSTEM

2.1 BACKGROUND

Regional Background

Central Argentina is home to the Pampean Plains (i.e., Pampas), a broad, low-relief region covered by vegetation-stabilized eolian silt- and sand-sized sediment of the Pampean Sand Sea (Zárate and Tripaldi, 2012; Garzanti et al., 2022). The Pampas are bordered on the west by the foothills of the Andes, the Chaco Plain and Sierras Pampeanas to the north, and the Atlantic Ocean on the east (Figure 1.1). The southern border of the Pampas coincides with northern Patagonia, with the Pampean Sand Sea extending as far south as the Rio Negro (Figure 1.1).

The Pampean Sand Sea extends approximately 800 km north to south and 400 km east to west with a total aerial coverage of 300,000 km^2 (Iriondo, 1997; Kröhling, 1999; Zárate and Tripaldi, 2012; Tripaldi et al., 2013). The loess belt adjacent to the Sand Sea extends approximately 800 km north to south with an approximate width of 200 km (Figure 1.1; Zárate and Tripaldi, 2012; Garzanti et al., 2022). Compositionally, the sand sea is comprised of mostly reworked quartz, feldspar, and volcanic glass (Teruggi, 1957; Zárate and Blasi, 1991; Iriondo, 1997) and was active during the last glacial maximum (Iriondo, 1997). Garzanti et al., (2022) also notes that the sediment becomes less rich in volcanic detritus to the north, reflecting decreased magmatism in the Sierras Pampeanas

portion of the Andes (Figure 1.1). The Sand Sea contains primarily longitudinal and parabolic dunes (Zárate and Tripaldi, 2012; Tripaldi et al., 2018; Garzanti et al., 2022). The formation of these dunes as well as the deposition of fine-grained sediment to the east and north of the sand sea indicates southwesterly and westerly winds during past glacial periods (Toggweiler et al., 2006; Iriondo 1997; Iriondo et al., 2009; Zárate and Tripaldi, 2012; Tripaldi et al., 2018).

The loess belt that surrounds the eastern portion of the Sand Sea has an average thickness of ~40 m (Imbellone and Teruggi, 1993; Iriondo, 1997; Zárate and Tripaldi, 2012) and contains sediments that have been reworked post-deposition (Teruggi, 1957). The loess belt contains mostly silt-sized grains of detrital quartz, plagioclase, K-feldspar, volcanic glass, and volcanoclastic lithics (Teruggi, 1957; Zárate and Fasano, 1989; Zárate and Blasi, 1991; Zárate and Blasi, 1993; Iriondo, 1997; Krohling 1999). There is a relatively high abundance of heavy minerals such as clinopyroxene, orthopyroxene, and amphibole (Teruggi, 1957; Zárate and Blasi, 1991, Garzanti et al., 2021a). On its eastward margin, the upper Pleistocene-Holocene loess belt overlies coastal cliffs along the Atlantic margin near Mar del Plata, Argentina (Zárate and Fasano, 1989).

Eolian sediments at the modern surface of the Pampas are late Pleistocene to Holocene in age (Kruck et al., 2011; Zárate and Tripaldi, 2012). Provenance data indicates the proto-sources of these sediments are in the Central and Southern Andes, as well as northern Patagonia (Garzanti et al., 2021a; Bruner et al., 2022). Underlying the late Pleistocene-Holocene sediments in the Pampas is the Cerro Azul Formation (Visconti et al., 2010; Folguera and Zárate, 2011; Nieto et al., 2017; Gutierrez et al., 2019), an upper Miocene unit composed of fluvial and eolian deposits (Prevosti et al.,

2021). The sediment in the Cerro Azul has similar detrital zircon U-Pb age distributions to the late Pleistocene-Holocene sediments, suggesting an eolian system approximating the late Pleistocene-Holocene system of the central Pampas started around 8 Ma during global late Miocene cooling (Stubbins et al., 2023). The unconformity separating the top of the Cerro Azul Formation and the overlying late-Pleistocene-Holocene deposits largely preclude the investigation of a continuous eolian provenance history using terrestrial deposits between the Late Miocene and Holocene. However, the loess deposits exposed along the eastern margin of central Argentina, as shown in red in Figure 1.1, were deposited during the Pliocene and Pleistocene and have the potential to fill in this knowledge gap.

Four major river systems feed into central Argentina that are particularly important for providing sediment to the eolian system (Figure 1.1; Zárate and Tripaldi, 2012; Garzanti et al., 2022; Bruner et al., 2022). In the north, the Río Paraná feeds into the northeastern margin of the Pampas in the loess/loessoid belt near Buenos Aires. The Río Desaguadero extends from the Central Andes and Sierras Pampeanas, flows along the western margin of the Pampas and ends in a terminal fan, although it likely extended to the Río Colorado during more humid climates (Garzanti et al., 2021a). The Ríos Colorado and Negro are located along the boundary between the Pampas and northern Patagonia and serve as important sources of sediment to the coastal plain and shelf all along the Atlantic margin of Argentina via longshore currents (Garzanti et al., 2021b). Detrital zircon data and heavy mineral assemblages also indicate that the Ríos Colorado and Negro contain distinguishable signatures compared to the river systems further north (Pepper et al., 2016; Garzanti et al., 2021b; Bruner et al., 2022).

Coastal Loess Deposits

Pliocene-Pleistocene loess and loessoid deposits are exposed along the Atlantic margin of central Argentina in coastal cliffs, which are 0–25 m high and extend for >30 km between the cities of Mar del Plata in the east and Miramar in the west (Figures 2.1, 2.2, 2.3). Calculations show the strata dip gently (< 3 degrees) to the west such that the lowermost units are exposed near Mar del Plata in the east and the uppermost units are exposed near Miramar (Figure 2.2). Although the base of the succession is not exposed, wells drilled in the area indicate the Pliocene-Pleistocene units unconformably overlie lower Paleozoic sandstones (M. Zárate, personal communication). As with other stratigraphic units in central Argentina, these coastal loess deposits were deposited in the Andean foreland basin system (Zárate and Tripaldi, 2012; Folguera et al., 2015; Tripaldi and Zárate, 2016). Isopachs of Neogene strata indicate the loess and loessoid units along the Argentinian coast were deposited within the back-bulge depozone, specifically (Folguera et al., 2015).

Zárate and Fasano (1989) present a thorough and detailed description of the lithology and stratigraphy of the strata in this area, dividing the deposits into 7 formations (Figure 2.2). The lowermost formation is the Chapadmalal Formation, a 10 m thick succession consisting of loess and reworked loessoid deposits including paleosols and fluvial channels. $^{40}Ar/^{39}Ar$ data from escoria at the lower and upper boundary of the Chapadmalal Formation indicate the unit was deposited between 3.74–3.04 Ma (Prevosti et al., 2021). Lithologically, it consists of mostly reddish-brown silty sand and paleosols with abundant mammal burrows (20 cm in diameter and up to 2 m in length; Zárate and

Fasano, 1989). Palms and grasses within the fossil fauna indicate the climate during the time of deposition was warmer than present (Prevosti et al., 2021).

A sharp erosional surface separates the Chapadmalal Formation from the overlying Barranca de los Lobos Formation (Figures 2.2, 2.3). The Barranca de los Lobos Formation contains fluvial channels 100s m wide at its base with paleosols and loess beds in the upper portion of the formation. The Barranca de los Lobos Formation is approximately 10 m thick and was deposited between 3.04–2.9 Ma (Cione and Tonni, 1995; Prevosti et al., 2021). The lower boundary is constrained by $^{40}Ar/^{39}Ar$ ages (Prevosti et al. 2021) and marks the start of the Marplatan South American Land Mammal Age (SALMA) Stage (Cione and Tonni, 1995).

The Barranca de los Lobos Formation is overlain by the Vorohué Formation, a 5 m thick succession deposited between 2.9 and 2.6 Ma (Figure 2.3; Zarate and Fasano, 1989; Cione and Tonni, 1995; Bidegain and Rico, 2012) based on South American land mammal fossils at the base and magnetostratigraphic data for the upper portion of the unit (Bidegain and Rico, 2012). The Vorohué Formation consists of channelized sandstone at the base, some with calcium carbonate nodules as well as loess, loessoid, and paleosol beds in the upper portion of the formation.

The San Andrés Formation overlies the Vorohué Formation along the southwestern section of the coastal cliffs (Figures 2.2, 2.3). The San Andrés Formation is approximately 0–5 m thick and was deposited between 2.6 and 1.78 Ma based on SALMA and magnetostratigraphic data (Zárate and Fasano, 1989; Cione and Tonni, 1995; Bidegain and Rico, 2012). The San Andrés Formation consists of silty claystone and loessoid beds with a rare occurrence of silty sandstone deposited in floodplain

environments (Zárate and Fasano, 1989). Due to the limited exposure or inaccessibility at the sampling sites, this unit was not sampled.

The overlying Miramar Formation is separated from the San Andrés Formation by an erosional surface (Figures 2.2, 2.3). The Miramar Formation is 5 m thick, with fluvial channels at the base, and is composed of sandstone and siltstone (Zárate and Fasano, 1989); silty paleosols and loess beds overlie the channel deposits. The Miramar Formation was deposited between 1.78–0.78 Ma based on measurements taken for magnetostratigraphic data (Orgeira, 1990, Bidegain and Rico, 2012).

The Arroyo Seco Formation overlies the Miramar Formation, is 0–5 m thick, and is separated from the underlying Miramar Formation by a thick carbonate bed found at the top of the Miramar Formation (Zárate and Fasano, 1989). The lower boundary of the Arroyo Seco Formation corresponds with the Matuyama and Brunes polarity boundary of the upper Miramar Formation (Orgeira, 1990; Bidegain and Rico, 2012); however, the exact age of the upper boundary of the Arroyo Seco Formation remains unclear.

The youngest unit in the area is the Santa Isabel Formation (Figure 2.3), a 1–3 m deposit composed of sandstone, siltstone, and clay with loess beds in the upper half of the formation. This unit is topped with modern soil (Zárate and Fasano, 1989). The Santa Isabel Formation was deposited above an erosional surface such that the underlying unit varies across the coastal cliffs. In the southwest, near the town of Miramar, the Santa Isabel overlies the Arroyo Seco, whereas in the northeast near the town of Mar del Plata, it overlies the Vorohué Formation (Figure 2.2; Zárate and Fasano, 1989). The lower depositional age boundary of the Arroyo Seco Formation corresponds with the upper age boundary of the Miramar Formation (0.78 Ma); however, the exact age between the

Arroyo Seco and Santa Isabel is unknown as both the Arroyo Seco and Santa Isabel fall in the magneto-stratigraphic Brunhes chron (Bidegain and Rico, 2012) as well as the SALMA Lujanian Stage (Zárate and Fasano, 1989). The upper boundary of the Santa Isabel is believed to be somewhere between 0.2 Ma and present (Zárate and Fasano, 1989).

2.2 METHODS

Nine samples of loessic sediment were collected at five sites along the coast of eastern Argentina between the towns of Miramar and Mar del Plata (Figure 2.1 locations A–E; Table 2.1). Stratigraphic sections were measured at the decimeter scale at each site. Roughly 3 kg samples were collected at each of the sites, with multiple samples in some locations. Samples were processed using standard mineral separation techniques at the University of South Carolina Rock Laboratory. Samples were disaggregated using a mortar and pestle and then run through a 1-mm sieve. Material <1mm in diameter was processed on a Gemini separating table. The heavy minerals from the Gemini processing were run through a 500-micron sieve followed by a Frantz magnetic separator at intensities of 0.3, 0.7, and 1.0 amps. Nonmagnetic grains were placed in heavy liquids to isolate the detrital zircons. Zircons within the samples do not have distinct or noticeable variations in size.

U-Th-Pb measurements were made at the University of Arizona LaserChron Center (ALC) using a Laser Ablation Multicollector Inductively-Coupled-Plasma Mass Spectrometer (LA-MC-ICPMS; Gehrels et. al 2008). The laser spot size used for the analyses was 25 μm except for a 30-μm spot size used for samples AS1 and SI2 due to the presence of larger zircons. Instrument drift, and elemental and mass biases were

corrected using the Sri Lanka (SL) and R33 zircon reference materials (Košler and Sylvester 2003; Paces and Miller, 1993; Black et al., 2004; Gehrels et al., 2008; Mattinson, 2010). Corrections for ages were made in-house using Microsoft Excel-based AgeCalc (Gehrels et al., 2008). $^{206}Pb/^{207}Pb$ was used to date zircon grains >900 Ma whereas $^{206}Pb/^{238}U$ was used for zircon grains <900 Ma. The rejection criteria are as follows: max $^{206}Pb/^{238}U$ error of 10%, max $^{206}Pb/^{207}Pb$ error of 10%, max discordance of 20%, and max reverse discordance of 10%. A detailed description of methods is included in the Appendix.

2.3 RESULTS

The Chapadmalal Formation is dominated by fine-grained silty sandstones between thin (<2 m) paleosols (Figure 2.4). The Barranca de los Lobos Formation contains a relatively even distribution of silt and fine-grained silty sandstone. The Vorohué Formation is slightly thinner in outcrop than the Chapadmalal and the Barranca de los Lobos, but contains a similar lithology to that of the Chapadmalal Formation. While no samples were collected in the San Andrés Formation due to the inaccessibility for sampling and poor likeliness of obtaining zircons, there was still a thin exposure of this formation in a layer of silt (Figure 2.4). The Miramar Formation is exposed closer to the town of Miramar (Figures 2.1, 2.2 and 2.4) and contains mostly very fine-grained silty sand with the presence of some very fine-grained lithic sandstones (Figure 2.4d). The Arroyo Seco Formation makes up the entirety of the measured section in Figure 2.4 (E) and is composed mostly of thinly bedded siltstone with carbonate nodules and fine-grained silty sandstone layers. The Santa Isabel Formation consists of mostly siltstone and was only exposed at two of the site locations (Figure 2.4). The exposures ranged

from one to two meters and laid unconformably over top of the Vorohué Formation in outcrop.

LA-MC-ICPMS yielded a total of *n*= 3941 ages fitting the filter parameters from the *N*= 9 samples (see Appendix for all raw data). Kernel Density Estimates (KDE) were constructed using best age from the U-Pb data to determine and compare age populations between samples. When the samples are combined, the detrital zircon U-Pb ages constitute several prominent U-Pb age populations (Figure 2.5a). The KDE was only constructed using zircon ages <2000 Ma resulting in *n*= 3899 zircons being used to construct the KDE in Figure 2.5a. The largest age modes in the combined dataset include 0–30 Ma, 60–120 Ma, 160–200 Ma, 240–290 Ma, 350–400 Ma, and 440–480 Ma, with relatively minor populations at 520–640 Ma and 960–1200 Ma.

Overall, the detrital zircon age populations in individual samples mirror those in the combined dataset (Figure 2.8). There is a prominent population of detrital zircons with ages from 0–30 Ma in all samples except for SI2 and MIR2; both of these samples contain the 0–30 Ma population but at low abundances (Figure 2.6). All samples have a population with ages of 60–120 Ma although the relative size of the population varies between samples. Similarly, a population of 160-200 Ma is present in all samples but to varying degrees. The largest age population in most samples includes zircons with ages of 240 - 290 Ma (Figure.2.8). Samples VOR2 and MIR2 contain detrital zircons with these ages but contain slight proportional differences in age populations.

Maximum Depositional Age

I calculated the maximum depositional age (MDA) for each sample based on the new detrital zircon data measured in this study. Detrital-zircon derived MDAs can be calculated in numerous ways (e.g., Coutts et al., 2019), with the best technique not always evident. For these units, I calculated using the methodology of the maximum likelihood algorithm outlined in Vermeesch (2021). Overall, the MDAs are consistent with the carefully assigned biostratigraphic, magnetostratigraphic, and $^{40}Ar/^{39}Ar$ ages of the studied units. Most importantly, none of the calculated MDAs are younger than the assigned ages of the coastal loess deposits. In general, the MDAs are either a few million years older than, or fall within, the constrained age range of the corresponding formation ages. Samples MIR2 and SI2 contain the oldest MDAs. The relatively old MDAs from both of these samples suggest a lack of young (<10 Ma) zircon grains available at the time of deposition, but little additional information can be deduced from these values.

Provenance of Zircon Grains:

The provenance of detrital zircon grains is interpreted by correlating the age populations within the sampled units to zircon U-Pb ages of potential source areas. Many of the source areas in the region have been characterized by previous investigators (e.g., Capaldi et al., 2017), and will be summarized here. Zircons with ages of 0–65 Ma are interpreted to be derived from the subduction-driven Andean magmatic arc, whose volcanic and intrusive rocks are exposed throughout the Andean Cordillera (Balgord, 2017; Capaldi et al., 2017; Bruner et al., 2022). Zircons with ages of 80–120 Ma are also interpreted to be derived from the Andean magmatic arc, but are more abundant in rivers

south of ~42 S latitude (e.g., Bruner et al., 2022). Detrital zircons with ages of 160–200 Ma are interpreted to be derived from igneous rocks associated with the Chon Aike Silicic igneous province, which is most widespread in Northern Patagonia (Pankhurst et al., 1998). Zircons with ages of 240–280 Ma are ubiquitous across central Argentina and are interpreted to be derived from the Permian-Triassic Choiyoi magmatic rocks, which extend from south-central South America to northern Patagonia (Sato et al., 2015; Luppo et al., 2018; Bastías-Mercado et al., 2020). Detrital zircons with ages of 330–400 Ma are interpreted to have been derived from rocks associated with a Carboniferous-age arc that formed on the western margin of Gondwana (Mpodozis and Kay, 1992; Sato et al., 2015; Naipauer et al., 2015; Capaldi et al., 2021). Zircons with ages of 440–480 Ma are interpreted to be derived from rocks associated with the Famatinian arc (Ramos, 2009) that formed during the Ordovician. Zircons between the ages of 500 and 540 Ma are derived from rocks associated with early magmatism in an area currently occupied by the Sierras Pampeanas during the start of the Famatinian Orogeny (Willner et al., 2008; Cristofolini et al., 2012). Detrital zircons with ages of 1000–1200 Ma are derived from rocks that crystalized during the Sunsas Orogeny (Bahlburg et al., 2009).

2.4 DISCUSSION

Comparing Coastal loess deposits to Pampean eolian deposits

The Pliocene-Pleistocene coastal loess deposits are restricted to a narrow band of outcrops and are absent within the Pampas, where the majority of eolian deposits in Argentina are located (Figure 1.1). As a result, it is unclear how the coastal loess deposits relate to the eolian deposits in the Pampas. Detrital zircon data from upper Pleistocene-

Holocene deposits in the Pampas of Argentina indicate the sediments were derived from sources in the Central and Southern Andes as well as northern Patagonia (Bruner et al., 2022). Detrital zircon data from the upper Miocene Cerro Azul Formation indicate a similar sediment provenance, indicating these deposits are the product of the same (or a very similar) eolian system that deposited the upper Pleistocene-Holocene sediments (Stubbins et al., 2023). However, the unconformity between the upper Miocene Cerro Azul Formation and the upper Pleistocene-Holocene deposits makes it difficult to assess if this eolian system was active during that time interval (e.g., Pliocene–mid-Pleistocene).

Figure 2.5 shows the combined KDE from the coastal loess deposits (A-red), the KDE from the combined upper Pleistocene-Holocene Pampean fluvial and eolian deposits (B-yellow; Bruner et al., 2022) and the combined loess and paleosol samples from the upper Miocene Cerro Azul Formation (C-Green; Stubbins et al., 2023). The grey bars in the figure represent ages where the KDEs contain major populations. With only minor exceptions, there is little difference in the populations between the samples. Both coastal loess deposits and upper Pleistocene-Holocene Pampean deposits (Bruner et al., 2022) contain large populations from 0–30 Ma, and from 240–290 Ma. The largest population in the Cerro Azul Formation (Stubbins et al., 2023) is also from 240–290 Ma. All three of the combined KDEs contain major peaks from 60–120 Ma, 160–200 Ma, 350–400 Ma, 440–480 Ma, 520–640 Ma, and minor yet noticeable populations at ca. 900 – 1200 Ma. The similarities in detrital zircon population peaks suggests that the coastal loess samples from this study are derived from the same sediment sources as the upper Pleistocene-Holocene deposits (Bruner et al. 2022) and the upper Miocene Cerro Azul Formation (Stubbins et al., 2023). We interpret these data to indicate that the eolian

system (e.g., sediment sources and transport pathways) responsible for the deposition of the Cerro Azul Formation and the upper Pleistocene-Holocene Pampean eolian sediments was also responsible for deposition of the Pliocene-Pleistocene coastal loess deposits in Argentina. While the similarities in combined KDEs from this study and Bruner et al. (2022) appear to be indisputable, there were two samples from Bruner et al. (2022) that were collected in extreme proximity (within 50 km) of the sample site that should be discussed in further detail. The individual KDEs for these two samples match closely in population peak proportions to samples MIR1, MIR2, and AS1, suggesting a near identical source.

Variability Between Coastal Loess Samples

All samples from the coastal loess deposits contain the same detrital zircon populations and, in many cases, the same relative proportions of detrital zircon grains (Figure 2.6). However, there are minor differences between samples that warrant further investigation. Figure 2.6 shows the individual KDEs for the nine samples in this study with the oldest sample from the Chapadmalal Formation on the bottom and the youngest samples from the Santa Isabel Formation on the top. The relative proportion of individual detrital zircon populations varies between each of the coastal loess deposits (Figure 2.6)—such stochastic variability is normal and provides little insight into longer-term sediment dynamics. Of greater interest are through-going trends that may reflect changes during the Pliocene-Pleistocene deposition of the coastal loess units. A first-order observation from Figure 2.6 suggests an overall change in the relative proportion of detrital zircons with ages from 40 and 220 Ma. Both KDEs and histograms show that the relative number of detrital zircons within this age range vary from relatively minor (e.g.,

CHAP1) to significant (e.g., MIR2), and are represented by two specific populations: 60–120 Ma and 160–200 Ma.

To examine the possibility of such a trend more objectively, we compare the relative percentage of grains with ages of 40–220 Ma from each sample, which includes the 60–120 and 160–200 Ma populations. Figure 2.7A shows the percentage of zircon grains in each sample with ages 40–220 Ma divided by the total number of zircons analyzed in the sample (multiplied by 100 to convert them into percent). These results support the hypothesized visual trends from the KDEs, specifically: 1) there is variability in the relative proportion of specific-aged zircon populations between samples; and 2) the lowermost deposits have lower percentages of 40–220 Ma grains compared to the uppermost deposits. Sample CHAP1 is the oldest sample in this study and it contains the fewest relative number of 40–220 Ma grains (22%), whereas sample MIR2 has the largest relative number of grains with these ages (34 %). Samples between the Chapadmalal Formation and the Miramar Formation display a rough trend from lower percentages of 40–220 Ma grains to higher percentages (23% to 30%), respectively. The three youngest samples, from the Arroyo Seco and Santa Isabel formations, contain percentages of 27% (Arroyo Seco), 27% (Santa Isabel 1) and 30% (Santa Isabel 2), which are less than the Miramar Formation (MIR2), but greater than the Chapadmalal Formation (CHAP1).

The importance of this observation is that zircons with ages between 40–220 Ma can be correlated to a specific portion of the adjacent Andes. Utilizing combined KDEs of zircons from potential source areas, zircons with these ages are associated with sources south of ~35 degrees S (Figure 2.9); for brevity I refer to this as the "southern source area." This is demonstrated by data from Pepper et al. (2016) and Bruner et al. (2022)

who compiled detrital zircon data from modern rivers in Bolivia and Argentina. Rivers flowing from the Andes of Bolivia and northern Argentina (i.e., “northern source area”), like the Río Deseguadero and Río Pilcomayo contain relatively large populations of detrital zircons with ages between ca. 250 and 700 Ma and few zircons with ages of 40–220 Ma (Figure 2.9). In contrast, detrital zircons with ages of 40–220 Ma are abundant in sediments transported by rivers exiting the Andes south of 35° S (Figure 2.10), like the Río Negro and Río Colorado.

To augment the riverine data in Pepper et al. (2016) and Bruner et al. (2022), we compiled detrital zircon U-Pb data from bedrock sources within the Andes. Two sediment source areas were created using the 35°S latitude as a boundary following the methodology and results from Bruner et al., 2022. The northern source area ranges from 29°S to 35 S and 71°W to 64°W and contains compiled data for *n*= 5,837 zircons (Thomas et al., 2004; Gleason et al., 2007; Casquet et al., 2008; Pankhurst et al., 2008; Willner et al., 2008; Mancuso et al., 2010; Morata et al., 2010; Rocha-Campos et al., 2011; Abre et al., 2012; Barredo et al., 2012; Dahlquist et al., 2013; Enkelmann et al., 2014; Levina et al., 2014; Ramacciotti et al., 2015; Horton and Fuentes, 2016; McKenzie et al., 2016; Capaldi et al., 2017;). The southern source area ranges from 35°S to 41°S and 71°W to 64°W and contains compiled data for *n*= 2,714 zircons (Pankhurst et al., 2006; Abre et al., 2011; Chernicoff et al., 2012; DiGiulio et al, 2012; Benedini and Gregori, 2013; Herve et al., 2013; Leanza et al., 2013; Horton and Fuentes, 2016; Balgord, 2017; Garcia Morabito et al., 2021).

North of 35°S latitude, there are 4 major age populations: 0–40 Ma; 220–360 Ma; 440–680 Ma; and 1000–1200 Ma. South of 35°S latitude, there are 5 major age

populations: 0–40 Ma; 40–120 Ma; 160–220 Ma; 240–340 Ma, and 340–420 Ma. These data are consistent with the interpretations from the fluvially-derived sediments compiled in Bruner et al., (2022) and provide corroborating evidence that zircons within the age range of 40–220 Ma are from south of 35° S in the central and southern section of the Andes. The Río Colorado and Río Negro are the most important conveyers of sediment to the Pampas and the Atlantic margin of Argentina south of 35° S (e.g., Garzanti et al., 2021b).

To better determine the percentage of sediment sourced from the two zones (northern versus southern source area), we examined the detrital zircon data from the coastal loess deposits with the detrital zircon unmixing model of Sundell and Saylor (2017). This model uses an inverse Monte Carlo approach to acquire the percentage of zircons from each given source. In practice, this means that if two sources are put into the model for an unknown, the two sources combined will account for 100% of zircons within the unknown sample. The model is run 10,000 times and uses only the top 1% (100) of trial runs. The ranking of the models is completed using a Kuiper V-Test (Kuiper, 1960). The model is also designed to ensure each potential sediment source is considered equally likely to be the most fruitful sediment source to the unknown sample, as it is impossible to know what the true source is before the analysis. The input error used for the following analysis was 2-sigma and Probability Density Plots (PDPs) were used as the chosen density distribution. The results for the following analyses are from the Cross-Correlation Coefficient test of the model.

Figure 2.7B shows the results of the unmixing model while comparing the individual samples to the compiled bedrock zircons database described above. The X-axis

is percent grains from the southern source zone while the Y-axis corresponds to the stratigraphic level from which the sample was collected (oldest on bottom, youngest on top). Overall, there is a similar trend between the modeling results (Figure 2.7B) and the percentage of grains between the ages of 40 and 220 Ma (Figure 2.7A). The contribution from southern source areas increases up section from sample CHAP1 to sample MIR2, followed by a slight decrease in the Arroyo Seco (AS1) and Santa Isabel (SI1 and SI2) samples; the uppermost sample from the Santa Isabel Formation contains a greater percentage from the southern source areas relative to the underlying sample (Figure 2.7B).

There is the potential for error using the bedrock compilation, most notably if there is a sampling bias for particular units or regions within the Andes. As an alternative test, we used the detrital zircon data from the major rivers in the region as potential sediment sources for the unmixing model (Figure 2.7c). The X-axis shows the percentage of grains derived from rivers in the south, the Y-axis shows the sample in the stratigraphic position. Like the results with the bedrock zircon database, the fluvial sources show there is a positive trend between samples CHAP1 and MIR2, followed by a relative decrease in the percentage from the south at sample AS1. The similarity in shape between all three of the graphs in Figure 2.7 indicates that the variability between samples is relatively consistent.

Ultimately, the data suggest a positive trend recording increased numbers of zircons with ages of 40–220 Ma from the older samples to the younger samples. The 40–220 Ma zircons are associated with sources from south of 35°S and correlate to sediment currently carried in the Ríos Colorado and Negro (Garzanti et al., 2021b).

Potential Drivers

The relative increase in detrital zircons from sediment sources south of 35° S in younger strata in the coastal loess deposits may be a product of evolving regional conditions. Because the Andes provide sediment for the Pliocene-Pleistocene coastal loess deposits, the vertical changes in detrital zircon provenance may be related to tectonic processes in the Andean orogen and Andean Foreland. However, based on compiled tectonic histories from the central and southern Andes, there are no clear correlations between tectonic events and changes in the detrital zircon U-Pb ages in the coastal loess deposits. Multiple studies indicate the adjacent Andes (the South-Central Cordillera and the Northern Patagonian Cordillera) had attained their current elevations before the Pliocene (Figure 2.9; Bissig et al., 2002; Ruskin and Jordan, 2007; Mathiasen and Premoli, 2010; Fosdick et al., 2011; Gutiérrez et al., 2013; Hoke et al., 2014; Levina et al., 2014; Martínez et al., 2015; Giambiagi et al., 2016; Giambiagi et al., 2017; Chang et al., 2019; Colwyn et al., 2019). Data indicating a changing elevation of the Andean Cordillera are limited, though there is no current evidence to suggest major elevation changes have occurred. Similarly, the initial deformation of foreland uplifts in central Argentina (e.g., Central Pampean Block) predate deposition of the Chapadmalal Formation (Folguera et al., 2015), and deformation has continued through the present day. I would expect to see an influx of sediment from North of 35° if the uplift of the Sierras Pampeanas, but the data show the opposite trend, suggesting that the uplifting block is not driving the shift in sedimentation. Similarly, it would be expected that drainage reorganization would be present with the uplifting block, but that also appears to be negligible in explaining the trend seen in the data because I would expect an increase

in sediment flowing from the South Central Andes to dominate the samples. No evidence indicates an increase in tectonic activity in the Andes south of 35° S relative to north of this latitude, which could be invoked to explain a greater influx from southern sources. Given the long history and complexity of deformation in the Andes, we cannot entirely exclude the possibility that surface uplift or exhumation in the Andes caused the observed changes in detrital zircon U-Pb ages; however, at this time there are no obvious tectonic events that can explain the changes observed in the detrital zircons within the coastal loess deposits.

In contrast to the tectonic history, global and regional climate have changed dramatically over the last 4 million years (Figure 2.9), with implications that could help to explain the trend in detrital zircon populations from the Chapadmalal Formation to the Santa Isabel Formation. Globally, the Pliocene Epoch is characterized by warm temperatures (relative to modern) that decrease over time, ultimately leading to the extensive glaciations of the Pleistocene (Taylor et al., 1993; Marlow et al., 2000; Ravelo et al., 2004; Rabassa et al., 2005; Lisiecki and Raymo, 2007; Sosidian and Rosenthal, 2009; Pagani et al., 2010; Elderfield et al., 2012; Federov et al., 2013; De Schepper et al., 2014; Karas et al., 2017; Peterson et al., 2020). The general cooling trend was interrupted by the mid-Pliocene warm period, which occurred between ca. 3.3 and 3.1 Ma (Raymo et al., 1996; Seki et al., 2010; Pagani et al., 2010; Haywood et al., 2016). Following the mid-Pliocene warm period, temperatures decreased into the early Pleistocene, with glacial-interglacial cycles occurring at ca. 40 ka (Rabassa et al., 2005; Lisiecki and Raymo, 2007; De Schepper et al., 2014) and sea-level fluctuations of greater amplitude (Miller et al., 2005; Rabassa et al., 2005). Particularly notable glaciations coincide with

cooling in the tropical oceans at 2.5 Ma, 2.1 Ma, and 1.7 Ma (Herbert et al., 2010). A shift from 40-ka glacial-interglacial cycles to 100-ka glacial-interglacial cycles occurred between approximately 1100 Ka and 900 Ka and continued through the remainder of the Pleistocene (Rutherford and D'Hondt, 2000; Lisiecki and Raymo, 2007; Bintanja and Van de Wal, 2008; Sosdian and Rosenthal, 2009; Lisiecki, 2010; Peterson et al., 2020).

Climate data specific to the Pampas and central Argentina are limited. Arguably the most complete climate record for southern South America comes from glacial till deposits in southern Patagonia (Figure 2.9), which is approximately 1500 km south of our study area. Because of this distance, these records cannot be used to constrain climate in central Argentina, but they are useful for examining general cooling/warming trends. There is evidence to suggest a glacial advance with isolated icecaps existing in the southern Patagonian Andes as far back as the late Pliocene (Rabassa et al., 2005; De Schepper et al., 2014). A series of glacial sediments were deposited between ca. 2.3 and 1.7 Ma followed by multiple tills deposited between 1.3 Ma and the Holocene (Rabassa et al., 2005; De Schepper et al., 2014).

The Chapadmalal Formation was deposited in the middle to late Pliocene, which is generally associated with warm global temperatures (Raymo et al., 1996; Seki et al., 2010; Pagani et al., 2010; Haywood et al., 2016) and sea-levels comparable to modern values (Miller et al., 2005). An exception to this is the period from 3.31 to 3.26, which corresponds to a period of glacial advances and ~60 m of sea-level drop during the Marine Isotope Stage “M2” (e.g., Tan et al., 2017). Just before this interval, there is evidence of glaciation in Patagonia marked by the presence of till deposits dated using K/Ar of underlying and overlying basalt flows as 3.55 Ma (Rabassa et al., 2005).

Additional glaciations are inferred in the region for the interval between 3.4 and 3.2 Ma (Rabassa et al., 2005). Following this was the mid-Pliocene warm period, which extended until approximately 3.1 Ma (Raymo et al., 1996; Seki et al., 2010; Pagani et al., 2010; Haywood et al., 2016). The Barranca de los Lobos Formation and Vorohué Formation were deposited between ca. 3.04 and 2.6 Ma during a period characterized by decreasing global temperatures (Marlow et al., 2000; Ravelo et al., 2004; Rabassa et al., 2005; Lisiecki and Raymo, 2007; Sosidian and Rosenthal, 2009; Pagani et al., 2010; Elderfield et al., 2012; Federov et al., 2013; De Schepper et al., 2014; Karas et al., 2017; Peterson et al., 2020).

The early Pleistocene is characterized by decreasing global temperatures and increased glaciations in the northern and southern hemispheres (Marlow et al., 2000; Lisiecki and Raymo, 2005; Lisiecki and Raymo, 2007; De Schepper et al., 2014). Thi interval in the coastal loess deposits is denoted by an unconformity that spans from 2.6 to 1.78 Ma (Figure 2.9). This period is coincident with numerous glacial till deposits in Southern Patagonia (Figure 2.9). The Miramar Formation was deposited between 1.78 and 0.78 Ma and contains the highest percentage of grains with ages of 40–220 Ma. During this interval of time, global temperatures continued to decrease and the periodicity of glacial-interglacial cycles shifted from 40-ka cycles to 100-ka cycles (Rutherford and D'Hondt, 2000; Lisiecki and Raymo, 2007; Bintanja and Van de Wal, 2008; Sosdian and Rosenthal, 2009; Lisiecki, 2010; Peterson et al., 2020) The Arroyo Seco and Santa Isabel formations were deposited <0.78 Ma coincident with decreasing global temperatures, increasing fluctuations in sea-level and glaciations in Patagonia (Lisiecki and Raymo, 2005; Miller et al., 2005; Rabassa et al., 2005).

Mechanisms for Changing DZ Signatures

The change in the relative proportion of 40–220 Ma zircons in the coastal loess deposit, which is interpreted as reflecting a greater relative input from sediment sources south of 35° S is the result of increased sediment flux from sources south of 35° S; decreased sediment flux from sources north of 35° S; or a combination of the two. The establishment of a paleo-Río Negro or Colorado during the late Pliocene-Pleistocene could explain the increase in sediment delivery to coastal regions during this time, as these river systems play a critical role in delivering sediment from the Andes to the coast (e.g., Garzanti et al., 2022). This is not considered a viable scenario, however, because the sedimentary evidence indicates fluvial systems have occupied the current flow paths of the Ríos Colorado and Negro since at least the late Miocene (Zavala & Freije, 2001; Melchor, 2009; Perez, 2013; Melchor et al., 2015; Stubbins, 2023). There are several other scenarios that we outline in the following discussion that provide plausible, but yet untested, mechanisms for changing the relative input from sediment sources north and south of 35° S.

Figure 2.10A depicts a late Pliocene-Pleistocene setting where cooler global temperatures result in equatorward (northward) migration of alpine glaciers in the Andes south of 35° S. The presence of glaciers in the mountains adjacent to the coastal loess deposits would result in increased sediment delivery fluxes from these sediment sources. There is a general correlation between glacial deposits in Patagonia (Rabassa et al., 2005) and the change in detrital zircon populations in our samples, although it is not particularly robust. Figure 2.10B depicts a late Pliocene-Pleistocene setting where falling sea-levels would expose the marine shelf south of the coastal loess deposits. In addition to the

sediment exposed on the shelf, falling sea levels would be accompanied by a basinward shift in the fluvial systems flowing to the coast. In this scenario, the exposed shelf and the east-flowing rivers would provide a new source of sediment from sources south of 35° S, which could be entrained by southerly and southwesterly winds. Iriondo and Garcia (1993) initially proposed this idea to explain the loess along the coastal margin of central Argentina. Rather than an increased sediment influx from sources south of 35° S, Figure 2.10C depicts an alternative scenario that involves a decrease in the influx of sediment coming from sediment sources north of 35° S. In this hypothesis, a decrease in the sediment flux from the Pampas to the coastal areas of Argentina leads to a relative increase in sediment from sources south of 35° S. The unconformity in the eolian strata in the Pampas suggests there was a period of sediment erosion, which may have ultimately removed material to a regional carbonate horizon known as the Tosca (Visconti et al., 2010; Gutierrez et al. 2019). Figure 2.10D depicts a scenario where previously existing Pliocene deposits are being scoured off by winds and blown to the coast of Argentina. The assumed increased humidity present along a coastal setting could act as a mechanism for the dust plume to settle. The settled dust would then make up a portion of the Pliocene deposit present along coastal Argentina today.

Table 2.1: Sample Information

Original sample names	Latitude	Longitude	Formation	Age of Formation (Ma)	New Sample Name	MDA (Ma)
21AR253	-38.154	-57.6198	Santa Isabel	? - 0.2/Present	SI2	10.00 +/- 0.95
21AR257	-38.1396	-57.6077	Santa Isabel	0.78 - ?	SI1	3.04 +/- 0.46
21AR249	-38.2941	-57.8492	Arroyo Seco	0.78 - ?	AS1	1.78 +/- 0.58
21AR261	-38.2197	-57.7113	Miramar	1.78 - 0.78	MIR2	10.73 +/- 0.74
21AR260	-38.2197	-57.7113	Miramat	1.78 - 0.78	MIR1	2.23 +/- 0.27
21AR258	-38.1797	-57.6496	Vorohué	2.9 - 2.6	VOR2	3.12 +/- 0.23
21AR256	-38.1396	-57.6077	Vorohué	2.9 - 2.6	VOR1	3.05 +/- 0.79
21AR255	-38.1396	-57.6077	Barranca de los Lobos	3.04 - 2.9	BDLL1	2.85 +/- 0.38
21AR254	-38.1396	-57.6077	Chapadmalal	3.74 - 3.04	CHAP1	4.04 +/ 0.39

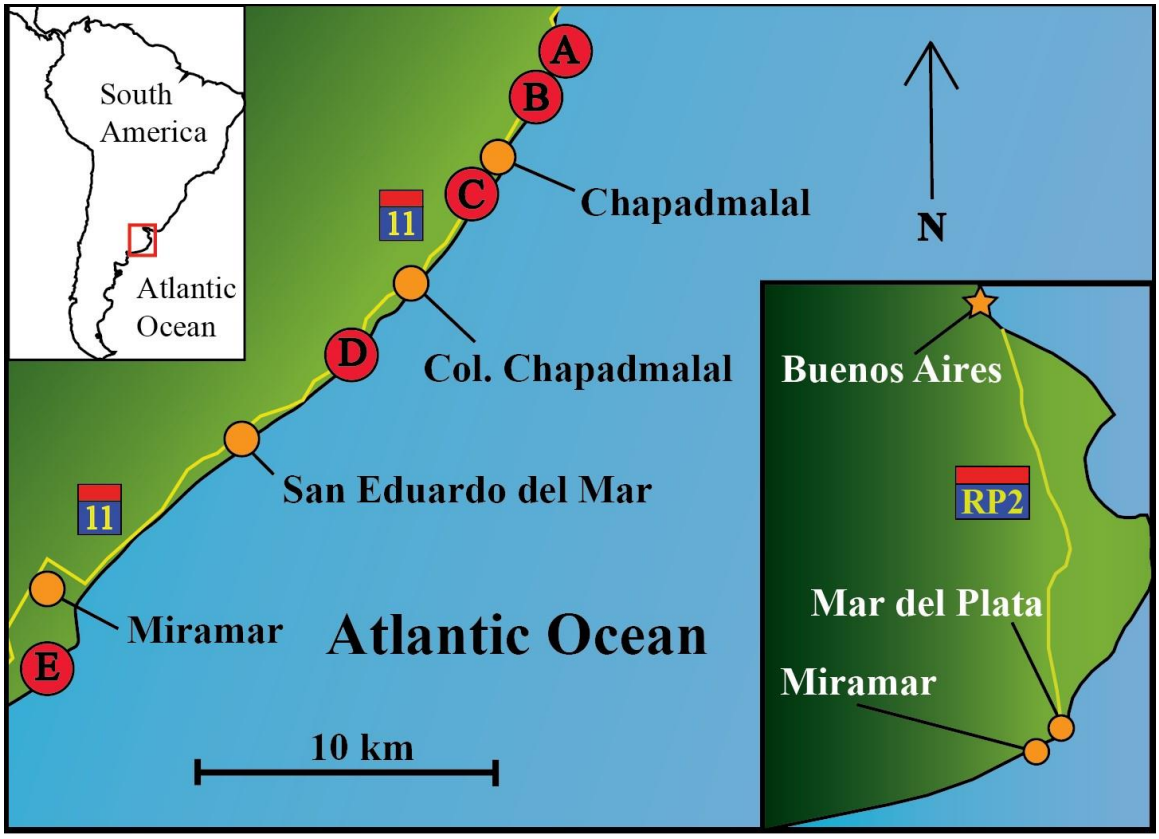

Figure 2.1: Local map denoting sample site locations for the coastal loess deposits. Cities and towns are labeled with orange circles and major roads (RP2 and 11) are labeled with yellow lines. Letters A-E correspond to sample site locations and will be referenced in later figures.

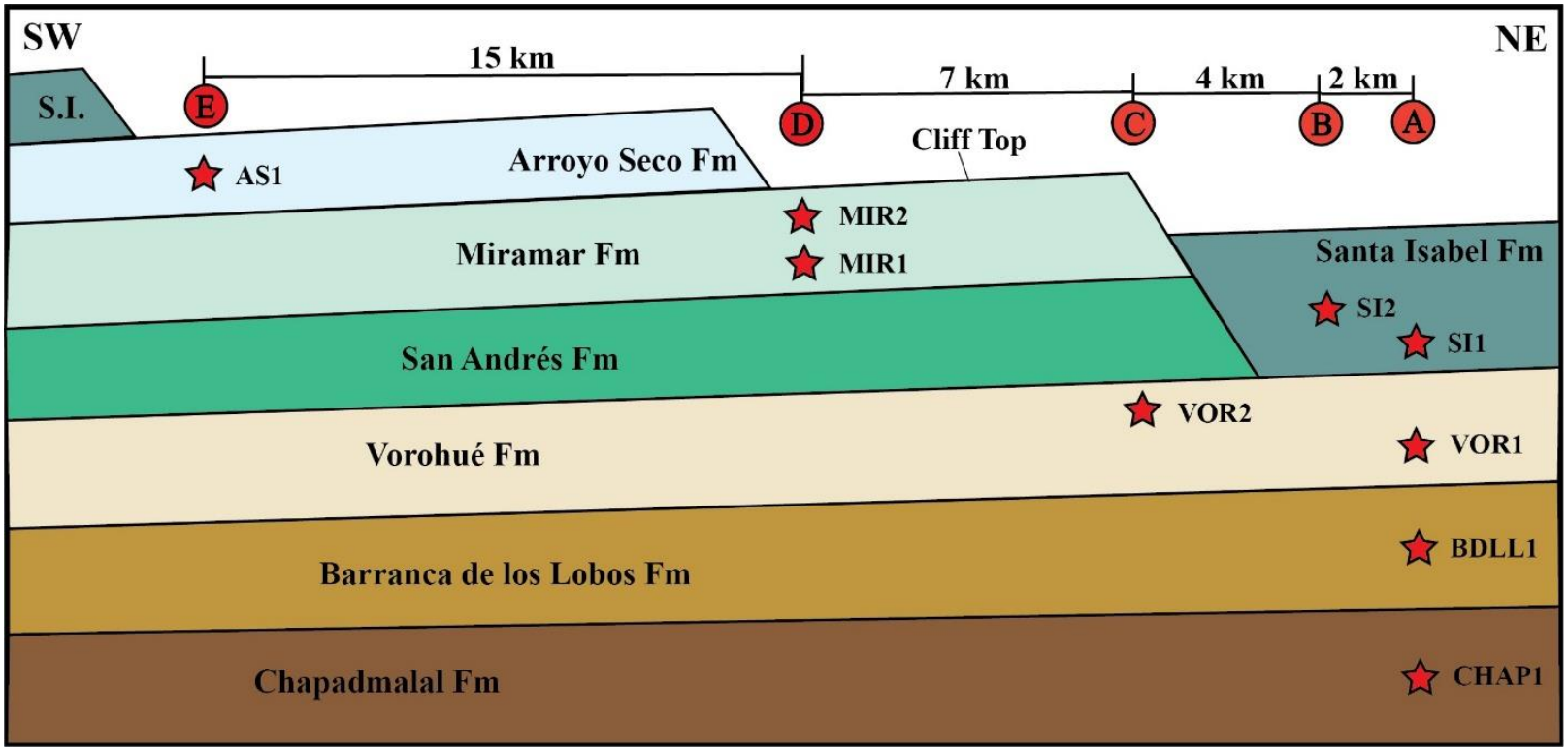

Figure 2.2: A schematic cross-section of the stratigraphy of the coastal loess deposits. The seven formations (from Zárate and Fasano, 1989) are shown dipping gently to the southwest. Not all formations were exposed along the coast. The thicknesses of the formations are not to scale. Letters A-E, as shown in Figure 2.1, represent the sample sites. Samples are shown by red stars.

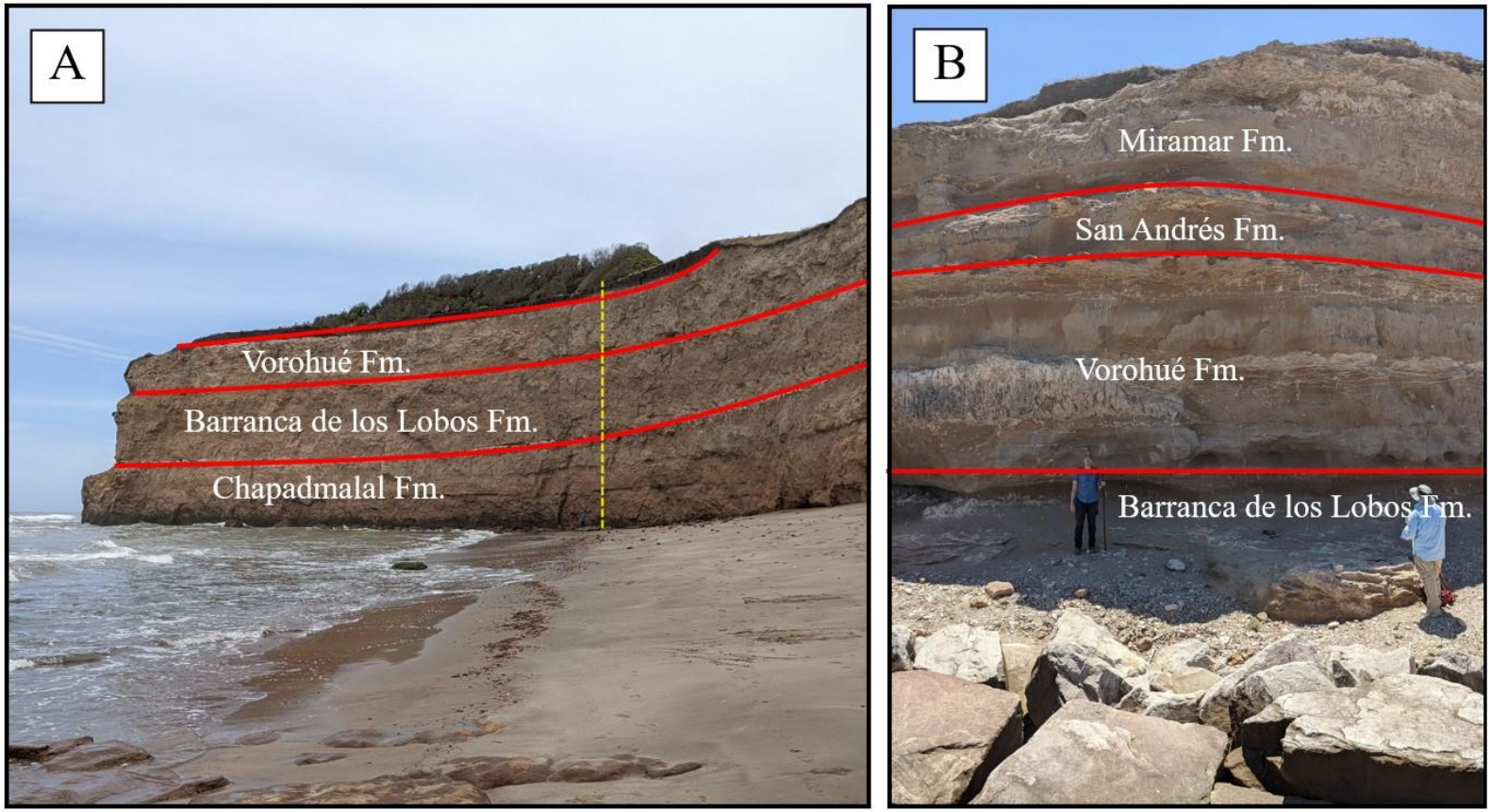

Figure 2.3: Annotated outcrop photos of the coastal cliffs. A. Chapadmalal, Barranca de los Lobos and Vorohué formations are shown. Yellow dashed marker is equal to ≈ 25 m. B. Barranca de los Lobos, Vorohué, San Andrés and Miramar formation, person for scale. Annotations follow the descriptions in Zárate and Fasano (1989).

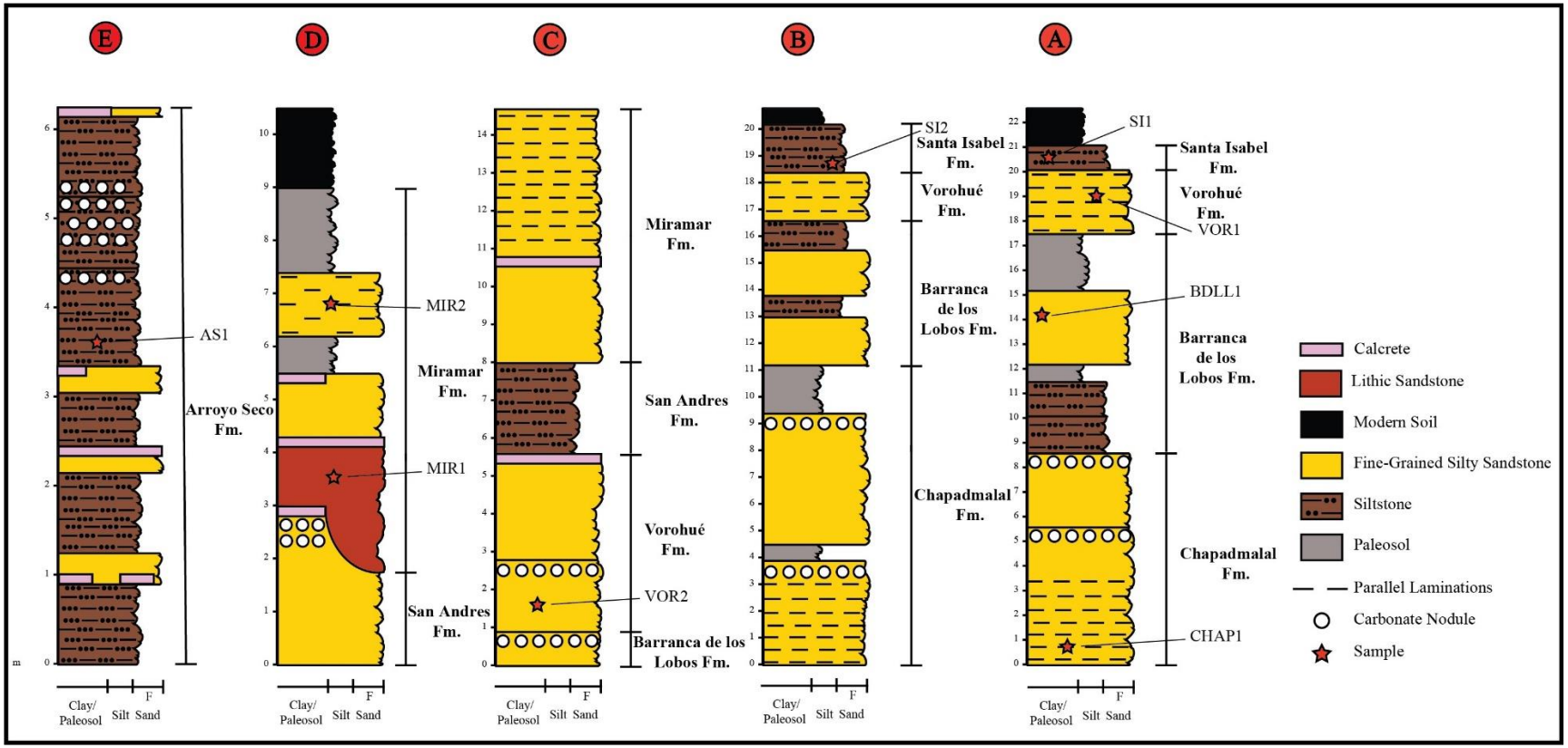

Figure 2.4: Measured sections from each of the sample sites, letters correspond to Figures. 2.1 and 2.2. Horizontal scale shows grain size, the vertical scale shows thickness, in meters. Note that the vertical scale differs between sections. Specific sampling location is denoted by red stars.

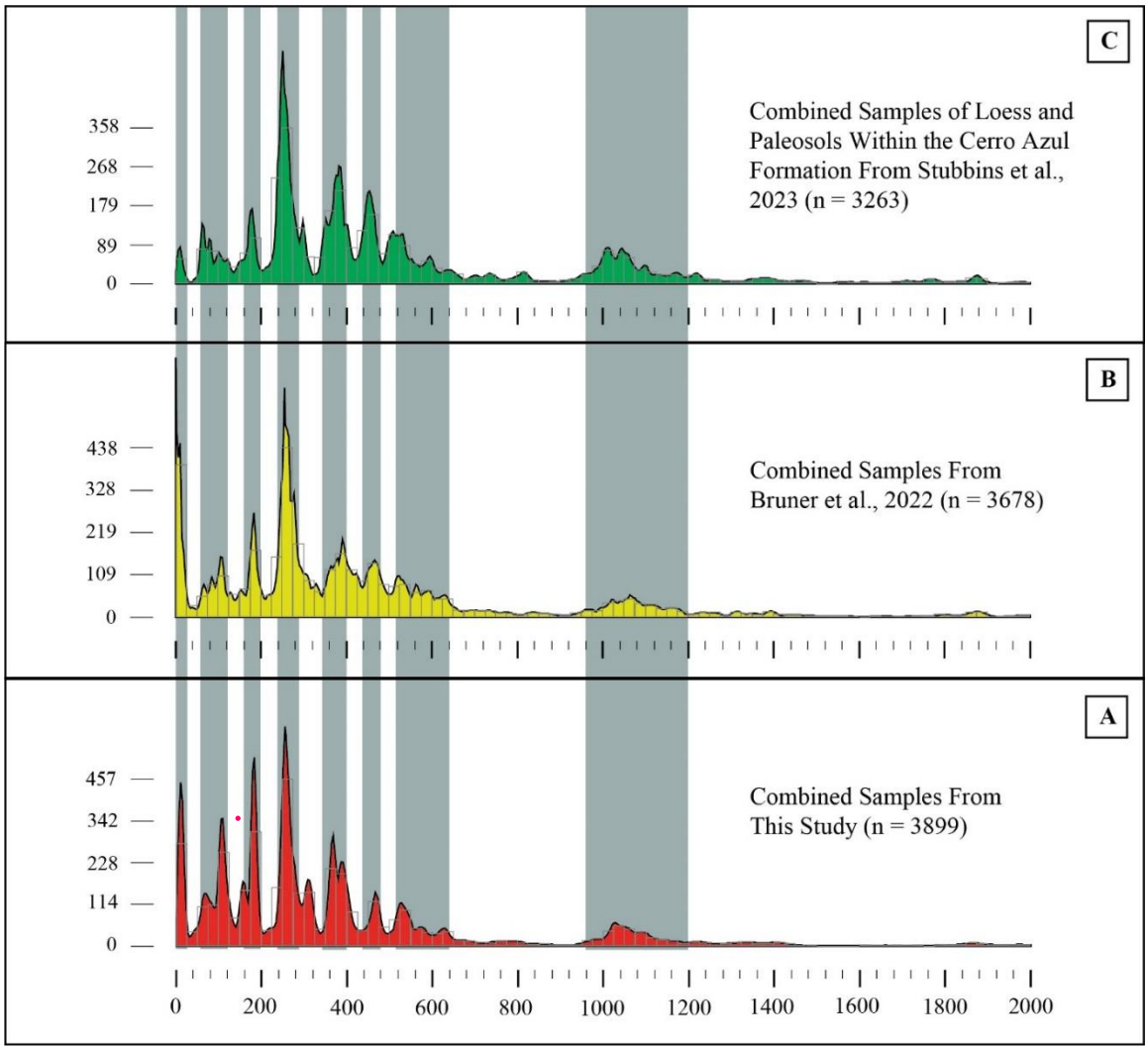

Figure 2.5: A. KDE of all samples from this study (red, A) – Numbers on the x axis are millions of years; B. KDE from loess, paleosol, river, and eolian sand samples from Bruner et al. (2022; yellow); and C. KDE from loess and paleosol samples from the upper Miocene Cerro Azul Formation from Stubbins et al. (2023; green). The grey rectangles represent major zircon age population peaks shared between all three KDEs. The numbers on the left are for the histogram bins, which were constructed with a binwidth of 25 myrs. The number of zircons above the age of 2000 Ma was minimal (n <100) and were therefore omitted from therefore not taken into account for the construction of the KDEs.

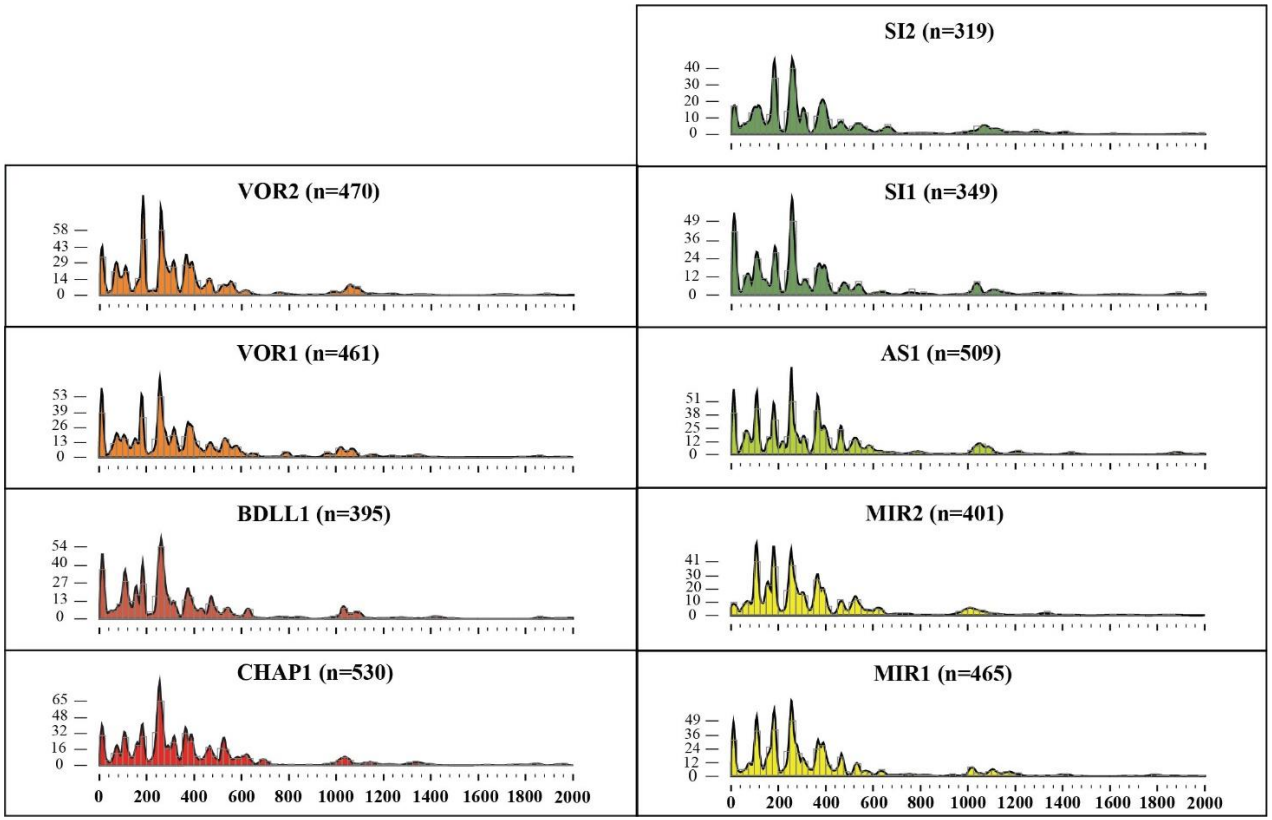

Figure 2.6: Individual KDEs from each sample in this study. The samples are ordered from oldest on the bottom (CHAP1) to youngest on top (SI1 and SI2). Numbers on X axis are millions of years, numbers on the left are for the histogram. The number of zircons above the age of 2000 Ma was minimal (<10 per sample) and were therefore omitted from the KDEs.

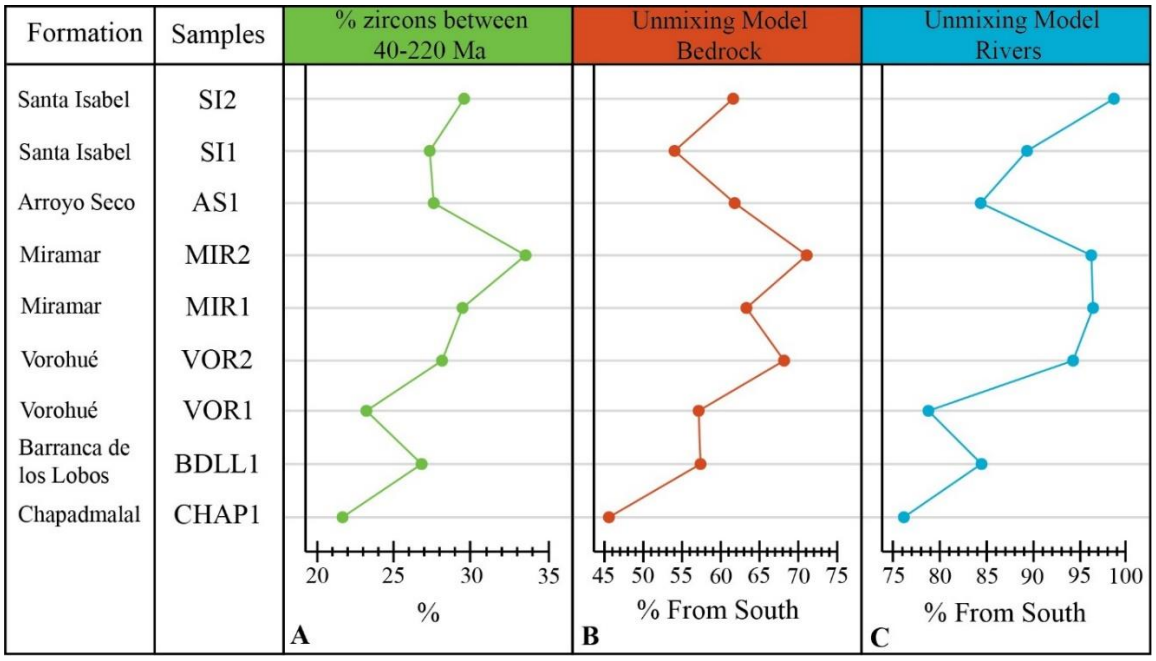

Figure 2.7: Figure showing the changes in: A) % zircons between 40 – 220 Ma for each sample; B) the unmixing model results using bedrock samples as sediment sources; and C) the unmixing model results using river samples as sediment sources (see text for references). Samples are ordered from oldest on bottom (CHAP1) to youngest on top (SI1 and SI2).

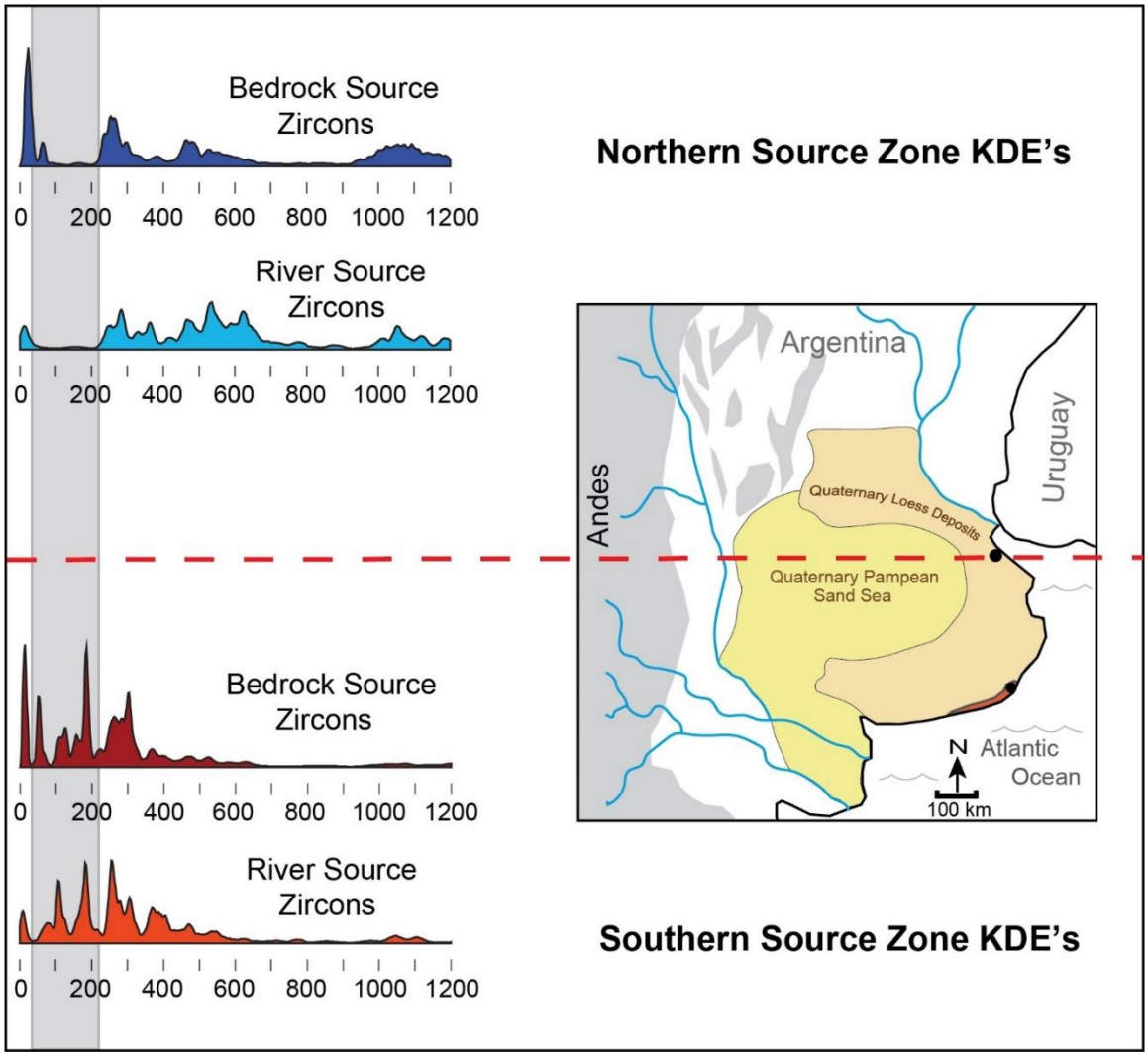

Figure 2.8: Potential source KDEs from the compiled bedrock and fluvial zircons (see text for references). The 35° S latitude line is marked with a red dashed line and represents the boundary between the "northern" and "southern" source zones. The darker colored KDEs are bedrock zircon data (see text) while the lighter KDEs are river zircon data (see text). The grey rectangle going through the KDEs highlights 40 – 220 Ma, which represents a difference between the two source areas.

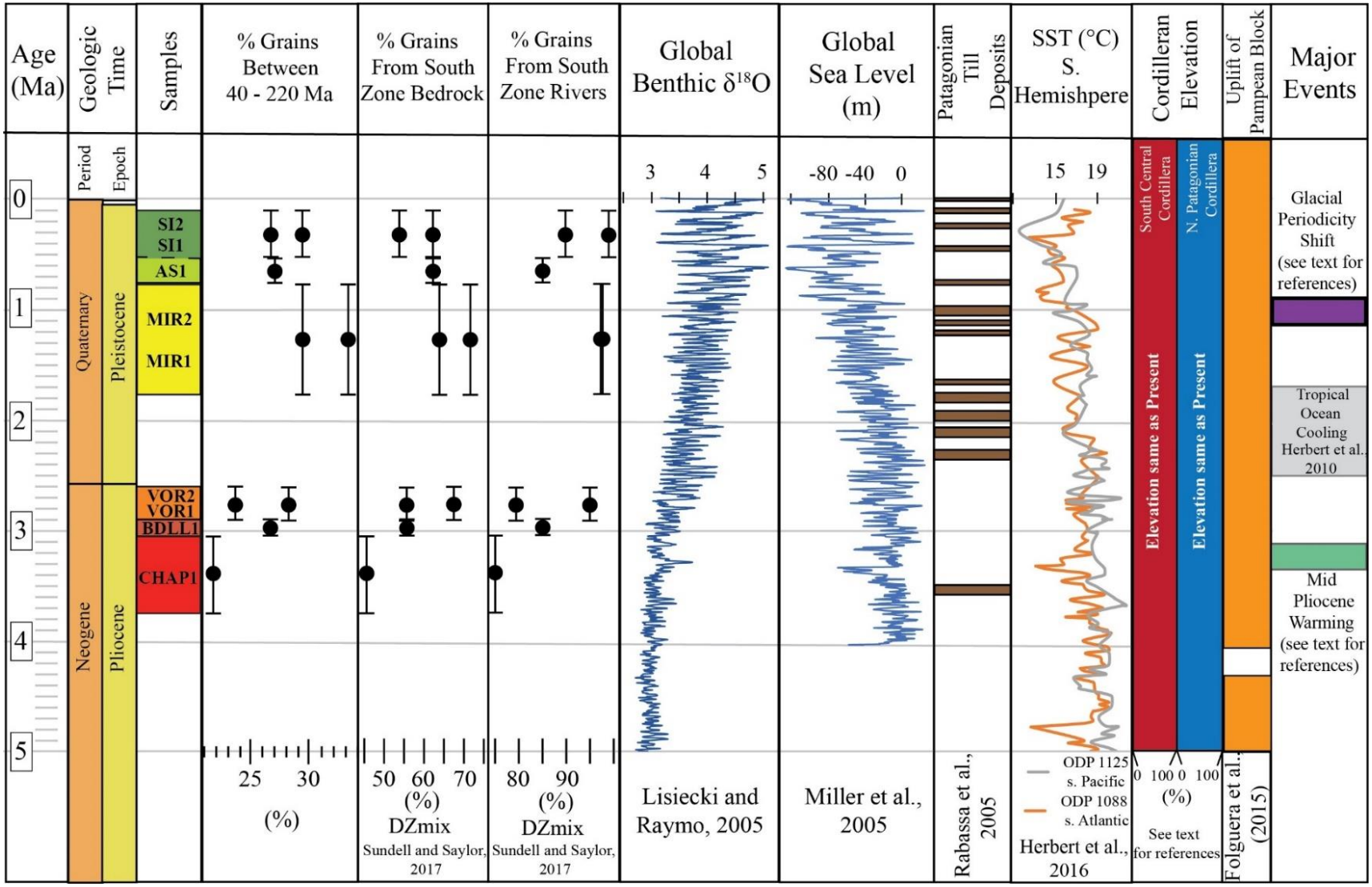
Age (Ma)
Geologic Time
Period
Epoch
Samples
% Grains Between 40 - 220 Ma
% Grains From South Zone Bedrock
% Grains From South Zone Rivers
Global Benthic δ18O
Global Sea Level (m)
Patagonian Till Deposits
SST (°C) S. Hemishpere
Cordilleran Elevation
Uplift of Pampean Block
Major Events
0
1
2
3
4
5
Quaternary
Neogene
Pleistocene
Pliocene
SI2
SI1
AS1
MIR2
MIR1
VOR2
VOR1
BDLL1
CHAP1
3 4 5
-80 -40 0
15 19
South Central Cordillera
N. Patagonian Cordillera
Elevation same as Present
Elevation same as Present
25 30
(%)
50 60 70
(%)
DZmix
Sundell and Saylor, 2017
80 90
(%)
DZmix
Sundell and Saylor, 2017
Lisiecki and Raymo, 2005
Miller et al., 2005
Rabassa et al., 2005
ODP 1125 s. Pacific
ODP 1088 s. Atlantic
Herbert et al., 2016
0 100 0 100
(%)
See text for references
Folguera et al., (2015)
Glacial Periodicity Shift (see text for references)
Tropical Ocean Cooling Herbert et al., 2010
Mid Pliocene Warming (see text for references)

Figure 2.9: The samples, as well as their potential depositional age ranges, the % grains 40 – 220 Ma within each sample (as discussed above to denote a more southern source), the DZmix results for bedrock and river sourced zircons, climate data, depositional data from glaciation, and tectonic data. The climate data presented is a stacked global benthic $\delta^{18}O$ (Lisiecki and Raymo, 2005), a global sea level curve obtained using eustatic sea level changes with oxygen isotopes as a proxy (Miller et al., 2005), and a Sea Surface Temperature (SST) curve using benthic oxygen isotopes as a proxy, with two offshore wells in the southern hemisphere (Herbert et al., 2016). Glacial till deposits in Patagonia as presented in Rabassa et al. (2005) are shown and are representative of periods of known glaciation in southern South America. Tectonic data is represented in the form of elevation of the South Central Cordillera and Northern Patagonian Cordillera compared to today. Figure 2.9 also shows the onset of deformation and uplift within the Pampean Block (Folguera et al., 2015). Note that the final elevation of the adjacent Cordilleras as well as the onset of activity within the Pampean Block all predate the deposition of the oldest sample in this study, suggesting a lack of evidence that the shift in provenance between samples is driven by tectonics.

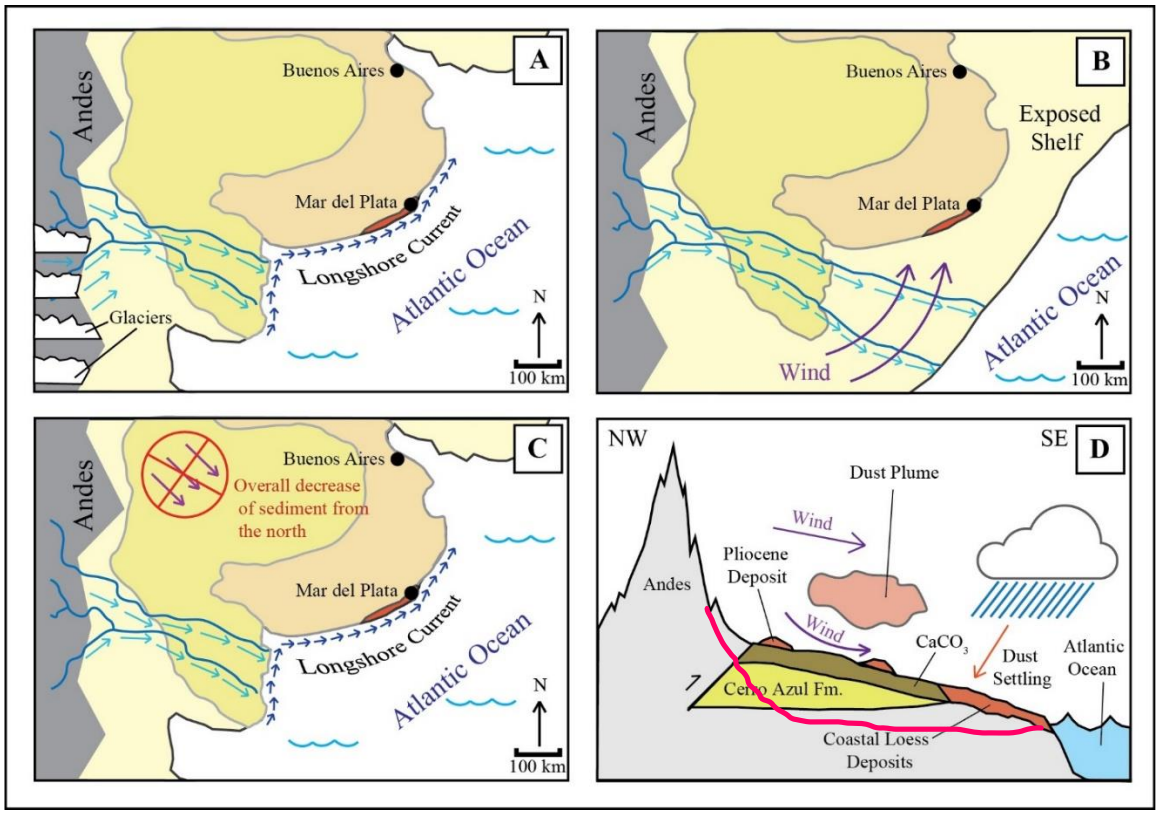

Figure 2.10: Potential scenarios explaining for the provenance trend seen in Figure 2.7. A) Depicts cooling conditions leading to northward migration of mountain glaciers, which would increase the sediment flux to the adjacent rivers and eventually the coast. B) Depicts a drop in sea level that exposes the continental shelf. The fluvial systems extend basinward to the new shoreline. The sediment on the exposed shelf and in the fluvial floodplains would be entrained by southwesterly winds (e.g., Toggweiler et al., 2006; Iriondo 1997; Iriondo et al., 2009; Zárate and Tripaldi, 2012; Tripaldi et al., 2018). C) Depicts decreased sediment influx from central Argentina. A decrease in sediment from central Argentina could result in the trends observed in figure 2.7. D) Depicts the scenario shown in C. Progressive erosion of sediment from central Argentina would occur until the widespread CaCO3 horizon is exposed. As all of the sediment from central Argentina is eroded, the relative influx from this area would decrease, leading to the trend observed in figure 2.7.

CHAPTER 3

CONCLUSION

Eolian sediments in central Argentina represent an important system by which dust is transferred to the South Atlantic Ocean, impacting the marine biology and possibly even CO_2 levels and global climate (Martin et al., 1990; Cassar et al., 2007; Martínez-Garcia et al., 2011; Mahowald et al., 2017). The coastal loess deposits exposed along the Atlantic margin of eastern-central Argentina were deposited during the Pliocene-Pleistocene (Zárate and Fasano, 1989; Orgeira, 1990; Cione and Tonni, 1995; Bidegain and Rico, 2012; Prevosti et al., 2021) and are some of the few units of that age in the entire region. The coastal loess deposits contain 7 notable and distinguishable zircon populations: 0–30 Ma, 60–120 Ma, 240–290 Ma, 350–400 Ma, 440–480 Ma, 520–640 Ma, 960–1200 Ma. The zircon populations within the Pliocene-Pleistocene coastal loess deposits closely resemble zircon populations of Miocene sediments found in Central Argentina (Stubbins et al., 2023) as well as late Pleistocene/Holocene sediments found throughout central and coastal Argentina (Bruner et al., 2022), suggesting the eolian system responsible for the sediment source, transport, and deposition of those deposits is the same system responsible for the source, transport, and deposition of the coastal loess deposits. The detrital zircon populations are very similar between individual samples from the coastal loess deposits, however, there is some variability present in the relative proportion of some specific age populations (60 – 120

Ma and 160 – 200 Ma) between samples. The variability in the number of grains within the age range of 40 – 220 Ma is interpreted to be a shift in relative sediment source from above and below 35° S. Ultimately, the samples display more of a "southern" input (relative increases in sediment from south of 35° S) through time followed by a slight decrease in "southern" sediment in the late Pleistocene. There are several hypotheses for what may drive this shift in sediment source relating to regional tectonics and climate, although no single hypothesis can be confirmed. There do not appear to be any major correlations with changing tectonics and the timing of deposition of the coastal loess deposits, leading us to believe that climate, which remained extremely dynamic from the mid Pliocene through the Pleistocene, may be the main driver causing this shift in sediment source through the Pliocene-Pleistocene. While it is hypothesized that climate may be the major driver causing the variability in sediment source seen in the coastal loess deposits, more data is needed to complete the picture.

REFERENCES

Abelmann, A., Gersonde, R., Cortese, G., Kuhn, G., & Smetacek, V. (2006). Extensive phytoplankton blooms in the Atlantic sector of the glacial Southern Ocean. *Paleoceanography*, *21*(1). https://doi.org/10.1029/2005PA001199

Abre, P., Cingolani, C. A., Cairncross, B., & Chemale, F. (2012). Siliciclastic Ordovician to Silurian units of the Argentine Precordillera: Constraints on provenance and tectonic setting in the proto-Andean margin of Gondwana. *Journal of South American Earth Sciences*, *40*, 1–22. https://doi.org/10.1016/j.jsames.2012.07.013

Abre, P., Cingolani, C., Zimmermann, U., Cairncross, B., & Chemale, F. (2011). Provenance of Ordovician clastic sequences of the San Rafael Block (Central Argentina), with emphasis on the Ponón Trehué Formation. *Gondwana Research*, *19*(1), 275–290. https://doi.org/10.1016/j.gr.2010.05.013

Bahlburg, H., Vervoort, J. D., Du Frane, S. A., Bock, B., Augustsson, C., & Reimann, C. (2009). Timing of crust formation and recycling in accretionary orogens: Insights learned from the western margin of South America. *Earth-Science Reviews*, *97*(1), 215–241. https://doi.org/10.1016/j.earscirev.2009.10.006

Balgord, E. A. (2017). Triassic to Neogene evolution of the south-central Andean arc determined by detrital zircon U-Pb and Hf analysis of Neuquén Basin strata, central Argentina (34°S–40°S). *Lithosphere*, *9*(3), 453–462. https://doi.org/10.1130/L546.1

Barredo, S., Chemale, F., Marsicano, C., Ávila, J. N., Ottone, E. G., & Ramos, V. A. (2012). Tectono-sequence stratigraphy and U–Pb zircon ages of the Rincón Blanco Depocenter, northern Cuyo Rift, Argentina. *Gondwana Research*, *21*(2), 624–636. https://doi.org/10.1016/j.gr.2011.05.016

Bastías-Mercado, F., González, J., & Oliveros, V. (2020). Volumetric and compositional estimation of the Choiyoi Magmatic Province and its comparison with other Silicic Large Igneous Provinces. *Journal of South American Earth Sciences*, *103*, 102749. https://doi.org/10.1016/j.jsames.2020.102749

Benedini, L., & Gregori, D. (2013). Significance of the Early Jurassic Garamilla formation in the western Nordpatagonian Massif. *Journal of South American Earth Sciences*, *45*, 259–277. https://doi.org/10.1016/j.jsames.2013.03.016

Bidegain, J. C., & Rico, Y. (2012). Magnetostratigraphy and magnetic parameters of a sedimentary sequence in Punta San Andres, Buenos Aires, Argentina. *Quaternary International*, *253*, 91–103. https://doi.org/10.1016/j.quaint.2011.08.018

Bintanja, R., & van de Wal, R. S. W. (2008). North American ice-sheet dynamics and the onset of 100,000-year glacial cycles. *Nature*, *454*(7206), Article 7206. https://doi.org/10.1038/nature07158

Bissig, T., Clark, A. H., Lee, J. K. W., & Hodgson, C. J. (2002). Miocene Landscape Evolution and Geomorphologic Controls on Epithermal Processes in the El Indio-Pascua Au-Ag-Cu Belt, Chile and Argentina. *Economic Geology*, *97*(5), 971–996. https://doi.org/10.2113/gsecongeo.97.5.971

Black, L. P., Kamo, S. L., Allen, C. M., Davis, D. W., Aleinikoff, J. N., Valley, J. W., Mundil, R., Campbell, I. H., Korsch, R. J., Williams, I. S., & Foudoulis, C. (2004).

Improved 206Pb/238U microprobe geochronology by the monitoring of a trace-element-related matrix effect; SHRIMP, ID–TIMS, ELA–ICP–MS and oxygen isotope documentation for a series of zircon standards. *Chemical Geology*, *205*(1), 115–140. https://doi.org/10.1016/j.chemgeo.2004.01.003

Bruner, A., Leier, A. L., Barbeau, D. L., Jr., Pullen, A., Fidler, M. K., & Stubbins, B. (2022). Detrital zircon provenance and transport pathways of Pleistocene-Holocene eolian sediment in the Pampean Plains, Argentina. *GSA Bulletin*, *135*(1–2), 435–448. https://doi.org/10.1130/B36267.1

Capaldi, T. N., Horton, B. K., McKenzie, N. R., Stockli, D. F., & Odlum, M. L. (2017). Sediment provenance in contractional orogens: The detrital zircon record from modern rivers in the Andean fold-thrust belt and foreland basin of western Argentina. *Earth and Planetary Science Letters*, *479*, 83–97. https://doi.org/10.1016/j.epsl.2017.09.001

Capaldi, T. N., McKenzie, N. R., Horton, B. K., Mackaman-Lofland, C., Colleps, C. L., & Stockli, D. F. (2021). Detrital zircon record of Phanerozoic magmatism in the southern Central Andes. *Geosphere*, *17*(3), 876–897. https://doi.org/10.1130/GES02346.1

Casquet, C., Pankhurst, R. J., Galindo, C., Rapela, C., Fanning, C. M., Baldo, E., Dahlquist, J., Casado, J. M. G., & Colombo, F. (2008). A deformed alkaline igneous rock–carbonatite complex from the Western Sierras Pampeanas, Argentina: Evidence for late Neoproterozoic opening of the Clymene Ocean? *Precambrian Research*, *165*(3), 205–220. https://doi.org/10.1016/j.precamres.2008.06.011

Cassar, N., Bender, M. L., Barnett, B. A., Fan, S., Moxim, W. J., Levy, H., & Tilbrook, B. (2007). The Southern Ocean Biological Response to Aeolian Iron Deposition. *Science*, *317*(5841), 1067–1070. https://doi.org/10.1126/science.1144602

Chang, Q., Hren, M. T., Brandon, M. T., Fosdick, J. C., VanderLeest, R. A., Bostelmann, J. E., & Ugalde, R. (2019). *Steady topography of Patagonian Andes through Cenozoic reconstructed by archives of precipitation hydrogen isotope composition*. *2019*, T41G-0343.

Chernicoff, C. J., Zappettini, E. O., Santos, J. O. S., Godeas, M. C., Belousova, E., & McNaughton, N. J. (2012). Identification and isotopic studies of early Cambrian magmatism (El Carancho Igneous Complex) at the boundary between Pampia terrane and the Río de la Plata craton, La Pampa province, Argentina. *Gondwana Research*, *21*(2), 378–393. https://doi.org/10.1016/j.gr.2011.04.007

Cione, A. L., & Tonni, E. P. (1995). Chronostratigraphy and "Land-Mammal Ages" in the Cenozoic of southern South America: Principles, practices, and the "Uquian" problem. *Journal of Paleontology*, *69*(1), 135–159. https://doi.org/10.1017/S0022336000026998

Colwyn, D. A., Brandon, M. T., Hren, M. T., Hourigan, J., Pacini, A., Cosgrove, M. G., Midzik, M., Garreaud, R. D., & Metzger, C. (2019). Growth and steady state of the Patagonian Andes. *American Journal of Science*, *319*(6), 431–472. https://doi.org/10.2475/06.2019.01

Coutts, D. S., Matthews, W. A., & Hubbard, S. M. (2019). Assessment of widely used methods to derive depositional ages from detrital zircon populations. *Geoscience Frontiers*, *10*(4), 1421–1435. https://doi.org/10.1016/j.gsf.2018.11.002

Cristofolini, E. A., Otamendi, J. E., Ducea, M. N., Pearson, D. M., Tibaldi, A. M., & Baliani, I. (2012). Detrital zircon U–Pb ages of metasedimentary rocks from Sierra de Valle Fértil: Entrapment of Middle and Late Cambrian marine successions in the deep roots of the Early Ordovician Famatinian arc. *Journal of South American Earth Sciences*, *37*, 77–94. https://doi.org/10.1016/j.jsames.2012.02.001

Dahlquist, J. A., Pankhurst, R. J., Gaschnig, R. M., Rapela, C. W., Casquet, C., Alasino, P. H., Galindo, C., & Baldo, E. G. (2013). Hf and Nd isotopes in Early Ordovician to Early Carboniferous granites as monitors of crustal growth in the Proto-Andean margin of Gondwana. *Gondwana Research*, *23*(4), 1617–1630. https://doi.org/10.1016/j.gr.2012.08.013

De Schepper, S., Gibbard, P. L., Salzmann, U., & Ehlers, J. (2014). A global synthesis of the marine and terrestrial evidence for glaciation during the Pliocene Epoch. *Earth-Science Reviews*, *135*, 83–102. https://doi.org/10.1016/j.earscirev.2014.04.003

Elderfield, H., Ferretti, P., Greaves, M., Crowhurst, S., McCave, I. N., Hodell, D., & Piotrowski, A. M. (2012). Evolution of Ocean Temperature and Ice Volume Through the Mid-Pleistocene Climate Transition. *Science*, *337*(6095), 704–709. https://doi.org/10.1126/science.1221294

Enkelmann, E., Ridgway, K. D., Carignano, C., & Linnemann, U. (2014). A thermochronometric view into an ancient landscape: Tectonic setting, development, and inversion of the Paleozoic eastern Paganzo basin, Argentina. *Lithosphere*, *6*(2), 93–107. https://doi.org/10.1130/L309.1

Fedorov, A. V., Brierley, C. M., Lawrence, K. T., Liu, Z., Dekens, P. S., & Ravelo, A. C. (2013). Patterns and mechanisms of early Pliocene warmth. *Nature*, *496*(7443), Article 7443. https://doi.org/10.1038/nature12003

Folguera, A., & Zárate, M. (2011). Neogene sedimentation in the Argentine foreland between 34°30'S and 41°S and its relation to the Andes evolution. *Cenozoic Geology of the Central Andes of Argentina*.

Folguera, A., Zárate, M., Tedesco, A., Dávila, F., & Ramos, V. A. (2015). Evolution of the Neogene Andean foreland basins of the Southern Pampas and Northern Patagonia (34°–41°S), Argentina. *Journal of South American Earth Sciences*, *64*, 452–466. https://doi.org/10.1016/j.jsames.2015.05.010

Fosdick, J. C., Romans, B. W., Fildani, A., Bernhardt, A., Calderón, M., & Graham, S. A. (2011). Kinematic evolution of the Patagonian retroarc fold-and-thrust belt and Magallanes foreland basin, Chile and Argentina, 51°30′S. *GSA Bulletin*, *123*(9–10), 1679–1698. https://doi.org/10.1130/B30242.1

García Morabito, E., Beltrán-Triviño, A., Terrizzano, C. M., Bechis, F., Likerman, J., Von Quadt, A., & Ramos, V. A. (2021). The Influence of Climate on the Dynamics of Mountain Building Within the Northern Patagonian Andes. *Tectonics*, *40*(2), e2020TC006374. https://doi.org/10.1029/2020TC006374

Garzanti, E., Capaldi, T., Tripaldi, A., Zárate, M., Limonta, M., & Vezzoli, G. (2022). Andean retroarc-basin dune fields and Pampean Sand Sea (Argentina): Provenance and drainage changes driven by tectonics and climate. *Earth-Science Reviews*, *231*, 104077. https://doi.org/10.1016/j.earscirev.2022.104077

Garzanti, E., Capaldi, T., Vezzoli, G., Limonta, M., & Sosa, N. (2021). Transcontinental retroarc sediment routing controlled by subduction geometry and climate change (Central and Southern Andes, Argentina). *Basin Research*, *33*(6), 3406–3437. https://doi.org/10.1111/bre.12607

Garzanti, E., Limonta, M., Vezzoli, G., & Sosa, N. (n.d.). *From Patagonia to Río de la Plata: Multistep long-distance littoral transport of Andean volcaniclastic sand along the Argentine passive margin—Garzanti—2021—Sedimentology—Wiley Online Library*. Retrieved February 14, 2024, from https://onlinelibrary.wiley.com/doi/full/10.1111/sed.12902

Gehrels, G. E., Valencia, V. A., & Ruiz, J. (2008). Enhanced precision, accuracy, efficiency, and spatial resolution of U-Pb ages by laser ablation–multicollector–inductively coupled plasma–mass spectrometry. *Geochemistry, Geophysics, Geosystems*, *9*(3). https://doi.org/10.1029/2007GC001805

Giambiagi, L., Mescua, J., Bechis, F., Hoke, G., Suriano, J., Spagnotto, S., Moreiras, S. M., Lossada, A., Mazzitelli, M., Dapoza, R. T., Folguera, A., Mardonez, D., & Pagano, D. S. (2016). Cenozoic Orogenic Evolution of the Southern Central Andes (32–36°S). In A. Folguera, M. Naipauer, L. Sagripanti, M. C. Ghiglione, D. L. Orts, & L. Giambiagi (Eds.), *Growth of the Southern Andes* (pp. 63–98). Springer International Publishing. https://doi.org/10.1007/978-3-319-23060-3_4

Giambiagi, L., Pamela Alvarez, P., Creixell, C., Mardonez, D., Murillo, I., Velasquez, R., Lossada, A., Suriano, J., Mescua, J., & Barrionuevo, M. (2017, October 26). *Cenozoic Shift From Compression to Strike-Slip Stress Regime in the High Andes at 30°S, During the Shallowing of the Slab: Implications for the El Indio/Tambo*

Mineral District—Giambiagi—2017—Tectonics—Wiley Online Library. https://agupubs.onlinelibrary.wiley.com/doi/full/10.1002/2017TC004608

Gleason, J. D., Finney, S. C., Peralta, S. H., Gehrels, G. E., & Marsaglia, K. M. (2007). Zircon and whole-rock Nd-Pb isotopic provenance of Middle and Upper Ordovician siliciclastic rocks, Argentine Precordillera. *Sedimentology*, *54*(1), 107–136. https://doi.org/10.1111/j.1365-3091.2006.00820.x

Gonzalez Bonorino, F. (1966). Soil clay mineralogy of the Pampa plains, Argentina. *Journal of Sedimentary Research*, *36*(4), 1026–1035. https://doi.org/10.1306/74D715EB-2B21-11D7-8648000102C1865D

Gutierrez, M., Escosteguy, L., & Espejo, P. (2019). Argentina Mining Geological Service, Institute of Geology and Mineral Resources. *Geological Sheet 3766-II*, *437*, 64.

Gutierrez, M., Escosteguy, L., & Espejo, P. (2019). Argentina Mining Geological Service, Institute of Geology and Mineral Resources. *Geological Sheet 3766-II*, *437*, 64.

Haywood, A. M., Dowsett, H. J., & Dolan, A. M. (2016). Integrating geological archives and climate models for the mid-Pliocene warm period. *Nature Communications*, *7*(1), Article 1. https://doi.org/10.1038/ncomms10646

Herbert, T. D., Peterson, L. C., Lawrence, K. T., & Liu, Z. (2010). Tropical Ocean Temperatures Over the Past 3.5 Million Years. *Science*, *328*(5985), 1530–1534. https://doi.org/10.1126/science.1185435

Hervé, F., Calderón, M., Fanning, C. M., Pankhurst, R. J., & Godoy, E. (2013). Provenance variations in the Late Paleozoic accretionary complex of central Chile as indicated by detrital zircons. *Gondwana Research*, *23*(3), 1122–1135. https://doi.org/10.1016/j.gr.2012.06.016

Hoke, G. D., Giambiagi, L. B., Garzione, C. N., Mahoney, J. B., & Strecker, M. R. (2014). Neogene paleoelevation of intermontane basins in a narrow, compressional mountain range, southern Central Andes of Argentina. *Earth and Planetary Science Letters*, *406*, 153–164. https://doi.org/10.1016/j.epsl.2014.08.032

Horton, B. K., & Fuentes, F. (2016). Sedimentary record of plate coupling and decoupling during growth of the Andes. *Geology*, *44*(8), 647–650. https://doi.org/10.1130/G37918.1

Imbellone, P. A., & Teruggi, M. E. (1993). Paleosols in loess deposits of the Argentine Pampas. *Quaternary International*, *17*, 49–55. https://doi.org/10.1016/1040-6182(93)90080-Y

Iriondo, M., Brunetto, E., & Kröhling, D. (2009). Historical climatic extremes as indicators for typical scenarios of Holocene climatic periods in the Pampean plain. *Palaeogeography, Palaeoclimatology, Palaeoecology*, *283*(3), 107–119. https://doi.org/10.1016/j.palaeo.2009.09.005

Iriondo, M. H. (1990). Map of the South American Plains—Its present state. In *Quaternary of South America and Antarctic Peninsula*. CRC Press.

Iriondo, M. H. (1997). Models of deposition of loess and loessoids in the upper quaternary of South America. *Journal of South American Earth Sciences*, *10*(1), 71–79. https://doi.org/10.1016/S0895-9811(97)00006-0

Iriondo, M. H., & Garcia, N. O. (1993). Climatic variations in the Argentine plains during the last 18,000 years. *Palaeogeography, Palaeoclimatology, Palaeoecology*, *101*(3), 209–220. https://doi.org/10.1016/0031-0182(93)90013-9

Karas, C., Nürnberg, D., Bahr, A., Groeneveld, J., Herrle, J. O., Tiedemann, R., & deMenocal, P. B. (2017). Pliocene oceanic seaways and global climate. *Scientific Reports*, *7*(1), Article 1. https://doi.org/10.1038/srep39842

Košler, J., & Sylvester, P. J. (2003). Present Trends and the Future of Zircon in Geochronology: Laser Ablation ICPMS. *Reviews in Mineralogy and Geochemistry*, *53*(1), 243–275. https://doi.org/10.2113/0530243

Kröhling, D. M. (1999). Sedimentological maps of the typical loessic units in North Pampa, Argentina. *Quaternary International*, *62*(1), 49–55. https://doi.org/10.1016/S1040-6182(99)00022-1

Kruck, W., Helms, F., Geyh, M. A., Suriano, J. M., Marengo, H. G., & Pereyra, F. (2011). Late Pleistocene-Holocene History of Chaco-Pampa Sediments in Argentina and Paraguay. *E&G Quaternary Science Journal*, *60*(1), 188–202. https://doi.org/10.3285/eg.60.1.13

Kuiper, N. H. (1960). Tests concerning random points on a circle. *Indagationes Mathematicae (Proceedings)*, *63*, 38–47. https://doi.org/10.1016/S1385-7258(60)50006-0

Leanza, H. A., Mazzini, A., Corfu, F., Llambías, E. J., Svensen, H., Planke, S., & Galland, O. (2013). The Chachil Limestone (Pliensbachian–earliest Toarcian) Neuquén Basin, Argentina: U–Pb age calibration and its significance on the Early Jurassic evolution of southwestern Gondwana. *Journal of South American Earth Sciences*, *42*, 171–185. https://doi.org/10.1016/j.jsames.2012.07.012

Levina, M., Horton, B. K., Fuentes, F., & Stockli, D. F. (2014, August 21). *Cenozoic sedimentation and exhumation of the foreland basin system preserved in the*

Precordillera thrust belt (31–32°S), southern central Andes, Argentina—Levina—2014—Tectonics—Wiley Online Library. https://agupubs.onlinelibrary.wiley.com/doi/full/10.1002/2013TC003424

Lisiecki, L. E. (2010). Links between eccentricity forcing and the 100,000-year glacial cycle. *Nature Geoscience*, *3*(5), Article 5. https://doi.org/10.1038/ngeo828

Lisiecki, L. E., & Raymo, M. E. (2005, January 18). *A Pliocene-Pleistocene stack of 57 globally distributed benthic δ18O records—Lisiecki—2005—Paleoceanography—Wiley Online Library*. https://agupubs.onlinelibrary.wiley.com/doi/full/10.1029/2004PA001071

Lisiecki, L. E., & Raymo, M. E. (2007). Plio–Pleistocene climate evolution: Trends and transitions in glacial cycle dynamics. *Quaternary Science Reviews*, *26*(1), 56–69. https://doi.org/10.1016/j.quascirev.2006.09.005

Luppo, T., López de Luchi, M. G., Rapalini, A. E., Martínez Dopico, C. I., & Fanning, C. M. (2018). Geochronologic evidence of a large magmatic province in northern Patagonia encompassing the Permian-Triassic boundary. *Journal of South American Earth Sciences*, *82*, 346–355. https://doi.org/10.1016/j.jsames.2018.01.003

Mahowald, N. M., Scanza, R., Brahney, J., Goodale, C. L., Hess, P. G., Moore, J. K., & Neff, J. (2017). Aerosol Deposition Impacts on Land and Ocean Carbon Cycles. *Current Climate Change Reports*, *3*(1), 16–31. https://doi.org/10.1007/s40641-017-0056-z

Mancuso, A. C., Chemale, F., Barredo, S., Ávila, J. N., Ottone, E. G., & Marsicano, C. (2010). Age constraints for the northernmost outcrops of the Triassic Cuyana Basin,

Argentina. *Journal of South American Earth Sciences*, *30*(2), 97–103. https://doi.org/10.1016/j.jsames.2010.03.001

Marlow, J. R., Lange, C. B., Wefer, G., & Rosell-Melé, A. (2000). Upwelling Intensification As Part of the Pliocene-Pleistocene Climate Transition. *Science*, *290*(5500), 2288–2291. https://doi.org/10.1126/science.290.5500.2288

Martin, J. H. (1990). Glacial-interglacial CO2 change: The Iron Hypothesis. *Paleoceanography*, *5*(1), 1–13. https://doi.org/10.1029/PA005i001p00001

Martin, J. H., & Fitzwater, S. E. (1988). Iron deficiency limits phytoplankton growth in the north-east Pacific subarctic. *Nature*, *331*(6154), Article 6154. https://doi.org/10.1038/331341a0

Martin, J. H., Fitzwater, S. E., & Gordon, R. M. (1990). Iron deficiency limits phytoplankton growth in Antarctic waters. *Global Biogeochemical Cycles*, *4*(1), 5–12. https://doi.org/10.1029/GB004i001p00005

Martínez, F., Arriagada, C., Valdivia, R., Deckart, K., & Peña, M. (2015). Geometry and kinematics of the Andean thick-skinned thrust systems: Insights from the Chilean Frontal Cordillera (28°–28.5°S), Central Andes. *Journal of South American Earth Sciences*, *64*, 307–324. https://doi.org/10.1016/j.jsames.2015.05.001

Martínez-Garcia, A., Rosell-Melé, A., Jaccard, S. L., Geibert, W., Sigman, D. M., & Haug, G. H. (2011). Southern Ocean dust–climate coupling over the past four million years. *Nature*, *476*(7360), Article 7360. https://doi.org/10.1038/nature10310

Mathiasen, P., & Premoli, A. C. (2010). Out in the cold: Genetic variation of Nothofagus pumilio (Nothofagaceae) provides evidence for latitudinally distinct evolutionary

histories in austral South America. *Molecular Ecology*, *19*(2), 371–385. https://doi.org/10.1111/j.1365-294X.2009.04456.x

Mattinson, J. M. (2010). Analysis of the relative decay constants of 235U and 238U by multi-step CA-TIMS measurements of closed-system natural zircon samples. *Chemical Geology*, *275*(3), 186–198. https://doi.org/10.1016/j.chemgeo.2010.05.007

McKenzie, N. R., Horton, B. K., Loomis, S. E., Stockli, D. F., Planavsky, N. J., & Lee, C.-T. A. (2016). Continental arc volcanism as the principal driver of icehouse-greenhouse variability. *Science*, *352*(6284), 444–447. https://doi.org/10.1126/science.aad5787

Melchor, R. N. (2009). Bird tracks preserved in fluvial channel facies of the Río Negro Formation (Neogene), La Pampa Province, Argentina. *Ameghiniana*, *46*(1), 209–214.

Melchor, R. N., Perez, M., Cardonatto, M. C., & Umazano, A. M. (2015). Late Miocene ground sloth footprints and their paleoenvironment*: Megatherichnum oportoi* revisited. *Palaeogeography, Palaeoclimatology, Palaeoecology*, *439*, 126–143. https://doi.org/10.1016/j.palaeo.2015.02.010

Miller, K. G., Kominz, M. A., Browning, J. V., Wright, J. D., Mountain, G. S., Katz, M. E., Sugarman, P. J., Cramer, B. S., Christie-Blick, N., & Pekar, S. F. (2005). The Phanerozoic Record of Global Sea-Level Change. *Science*, *310*(5752), 1293–1298. https://doi.org/10.1126/science.1116412

Morata Céspedes, D., Castro de Machuca, B., Arancibia, G., Pontoriero, S., & Fanning, M. (2010). *Peraluminous Grenvillian TTG in the Sierra de Pie de Palo, Western*

Sierras Pampeanas, Argentina: Petrology, geochronology, geochemistry and petrogenetic implications. https://doi.org/10.1016/j.precamres.2010.01.001

MPODOZIS, C., & KAY, S. M. (1992). Late Paleozoic to Triassic evolution of the Gondwana margin: Evidence from Chilean Frontal Cordilleran batholiths (28°S to 31°S). *GSA Bulletin*, *104*(8), 999–1014. https://doi.org/10.1130/0016-7606(1992)104<0999:LPTTEO>2.3.CO;2

Naipauer, M., Tapia, F., Mescua, J., Farías, M., Pimentel, M. M., & Ramos, V. A. (2015). Detrital and volcanic zircon U–Pb ages from southern Mendoza (Argentina): An insight on the source regions in the northern part of the Neuquén Basin. *Journal of South American Earth Sciences*, *64*, 434–451. https://doi.org/10.1016/j.jsames.2015.09.013

Nieto, S., Espejo, P., Chernicoff, C., & Zappetini, E. (n.d.). Geological Sheet 3766-IV, General Acha. Province of La Pampa. *Institute of Geology and Resources Minerals, Argentine Mining Geological Service. Bulletin 427*.

Orgeira, M. J. (1990). Palaeomagnetism of late Cenozoic fossiliferous sediments from Barranca de los Lobos (Buenos Aires Province, Argentina). The magnetic age of the South American land-mammal ages. *Physics of the Earth and Planetary Interiors*, *64*(2), 121–132. https://doi.org/10.1016/0031-9201(90)90032-S

Paces, J. B., & Miller Jr., J. D. (1993). Precise U-Pb ages of Duluth Complex and related mafic intrusions, northeastern Minnesota: Geochronological insights to physical, petrogenetic, paleomagnetic, and tectonomagmatic processes associated with the 1.1 Ga Midcontinent Rift System. *Journal of Geophysical Research: Solid Earth*, *98*(B8), 13997–14013. https://doi.org/10.1029/93JB01159

Pagani, M., Liu, Z., LaRiviere, J., & Ravelo, A. C. (2010). High Earth-system climate sensitivity determined from Pliocene carbon dioxide concentrations. *Nature Geoscience*, *3*(1), Article 1. https://doi.org/10.1038/ngeo724

Pankhurst, R. J., Leat, P. T., Sruoga, P., Rapela, C. W., Márquez, M., Storey, B. C., & Riley, T. R. (1998). The Chon Aike province of Patagonia and related rocks in West Antarctica: A silicic large igneous province. *Journal of Volcanology and Geothermal Research*, *81*(1), 113–136. https://doi.org/10.1016/S0377-0273(97)00070-X

Pankhurst, R. J., Rapela, C. W., Fanning, C. M., & Márquez, M. (2006). Gondwanide continental collision and the origin of Patagonia. *Earth-Science Reviews*, *76*(3), 235–257. https://doi.org/10.1016/j.earscirev.2006.02.001

Pankhurst, R. J., Rapela, C. W., Galindo, C., Alasino, P., Fanning, M., Saavedra, J., & Baldo, E. G. (2008). New SHRIMP U-Pb data from the Famatina Complex: Constraining Early–Mid Ordovician Famatinian magmatism in the Sierras Pampeanas, Argentina. *Geologica Acta*, 319–333.

Pepper, M., Gehrels, G., Pullen, A., Ibanez-Mejia, M., Ward, K. M., & Kapp, P. (2016). Magmatic history and crustal genesis of western South America: Constraints from U-Pb ages and Hf isotopes of detrital zircons in modern rivers. *Geosphere*, *12*(5), 1532–1555. https://doi.org/10.1130/GES01315.1

Peterson, L. C., Lawrence, K. T., Herbert, T. D., Caballero-Gill, R., Wilson, J., Huska, K., Miller, H., Kelly, C., Seidenstein, J., Hovey, D., & Holte, L. (2020). *Plio-Pleistocene Hemispheric (A)Symmetries in the Northern and Southern Hemisphere Midlatitudes—Peterson—2020—Paleoceanography and Paleoclimatology—Wiley*

Online Library. https://agupubs.onlinelibrary.wiley.com/doi/full/10.1029/2019PA003720

Prevosti, F. J., Romano, C. O., Forasiepi, A. M., Hemming, S., Bonini, R., Candela, A. M., Cerdeño, E., Madozzo Jaén, M. C., Ortiz, P. E., Pujos, F., Rasia, L., Schmidt, G. I., Taglioretti, M., MacPhee, R. D. E., & Pardiñas, U. F. J. (2021). New radiometric 40Ar–39Ar dates and faunistic analyses refine evolutionary dynamics of Neogene vertebrate assemblages in southern South America. *Scientific Reports*, *11*(1), Article 1. https://doi.org/10.1038/s41598-021-89135-1

Rabassa, J., Coronato, A. M., & Salemme, M. (2005). Chronology of the Late Cenozoic Patagonian glaciations and their correlation with biostratigraphic units of the Pampean region (Argentina). *Journal of South American Earth Sciences*, *20*(1), 81–103. https://doi.org/10.1016/j.jsames.2005.07.004

Ramacciotti, C. D., Baldo, E. G., & Casquet, C. (2015). U–Pb SHRIMP detrital zircon ages from the Neoproterozoic Difunta Correa Metasedimentary Sequence (Western Sierras Pampeanas, Argentina): Provenance and paleogeographic implications. *Precambrian Research*, *270*, 39–49. https://doi.org/10.1016/j.precamres.2015.09.008

Ramos, V. A. (n.d.). *Backbone of the Americas: Shallow Subduction, Plateau Uplift, and Ridge and ... - Google Books*. Retrieved February 14, 2024, from https://books.google.com/books?hl=en&lr=&id=ThpUlnCKwdgC&oi=fnd&pg=PA31&dq=Ramos,+V.+A.+(2009).+Anatomy+and+global+context+of+the+Andes:+Main+geologic+features+and+the+Andean+orogenic+cycle.+In+S.+M.+Kay,+V.+A.+Ramos,+%26+W.+R.+Dickinson,+Backbone+of+the+Americas:+Shallow+Sub

duction,+Plateau+Uplift,+and+Ridge+and+Terrane+Collision.+Geological+Society+of+America.+https://doi.org/10.1130/2009.1204(02)&ots=X1tkMOl9Es&sig=9JK6O_JaSH3GrOSNgqVVqUVdjQI#v=onepage&q&f=false

Ravelo, A. C., Andreasen, D. H., Lyle, M., Olivarez Lyle, A., & Wara, M. W. (2004). Regional climate shifts caused by gradual global cooling in the Pliocene epoch. *Nature*, *429*(6989), Article 6989. https://doi.org/10.1038/nature02567

Raymo, M. E., Grant, B., Horowitz, M., & Rau, G. H. (1996). Mid-Pliocene warmth: Stronger greenhouse and stronger conveyor. *Marine Micropaleontology*, *27*(1), 313–326. https://doi.org/10.1016/0377-8398(95)00048-8

Rocha-Campos, A. C., Basei, M. A., Nutman, A. P., Kleiman, L. E., Varela, R., Llambias, E., Canile, F. M., & da Rosa, O. de C. R. (2011). 30 million years of Permian volcanism recorded in the Choiyoi igneous province (W Argentina) and their source for younger ash fall deposits in the Paraná Basin: SHRIMP U–Pb zircon geochronology evidence. *Gondwana Research*, *19*(2), 509–523. https://doi.org/10.1016/j.gr.2010.07.003

Ruskin, B. G., & Jordan, T. E. (2007). Climate Change Across Continental Sequence Boundaries: Paleopedology and Lithofacies of Iglesia Basin, Northwestern Argentina. *Journal of Sedimentary Research*, *77*(9), 661–679. https://doi.org/10.2110/jsr.2007.069

Rutherford, S., & D'Hondt, S. (2000). Early onset and tropical forcing of 100,000-year Pleistocene glacial cycles. *Nature*, *408*(6808), Article 6808. https://doi.org/10.1038/35040533

Sato, A. M., Llambías, E. J., Basei, M. A. S., & Castro, C. E. (2015). Three stages in the Late Paleozoic to Triassic magmatism of southwestern Gondwana, and the relationships with the volcanogenic events in coeval basins. *Journal of South American Earth Sciences*, *63*, 48–69. https://doi.org/10.1016/j.jsames.2015.07.005

Seki, O., Foster, G. L., Schmidt, D. N., Mackensen, A., Kawamura, K., & Pancost, R. D. (2010). Alkenone and boron-based Pliocene *p*CO2 records. *Earth and Planetary Science Letters*, *292*(1), 201–211. https://doi.org/10.1016/j.epsl.2010.01.037

Sosdian, S., & Rosenthal, Y. (2009). Deep-Sea Temperature and Ice Volume Changes Across the Pliocene-Pleistocene Climate Transitions. *Science*, *325*(5938), 306–310. https://doi.org/10.1126/science.1169938

Stubbins, B., Leier, A. L., Barbeau, D. L., Pullen, A., Abell, J. T., Nie, J., Zárate, M. A., & Fidler, M. K. (2023). Global climate forcing on late Miocene establishment of the Pampean aeolian system in South America. *Nature Communications*, *14*(1), Article 1. https://doi.org/10.1038/s41467-023-42537-3

Stubbins, B. M. (2023). *Dust Production and Transport in a Long-Lived Fluvial-Eolian System in the Pampas of South America* [M.S., University of South Carolina]. https://www.proquest.com/docview/2841249182/abstract/B5B92F0BCD6A404EPQ/1

Sundell, K. E., & Saylor, J. E. (n.d.). *Unmixing detrital geochronology age distributions—Sundell—2017—Geochemistry, Geophysics, Geosystems—Wiley Online Library*. Retrieved February 14, 2024, from https://agupubs.onlinelibrary.wiley.com/doi/full/10.1002/2016GC006774

Tan, N., Ramstein, G., Dumas, C., Contoux, C., Ladant, J.-B., Sepulchre, P., Zhang, Z., & De Schepper, S. (2017). Exploring the MIS M2 glaciation occurring during a warm and high atmospheric CO2 Pliocene background climate. *Earth and Planetary Science Letters*, *472*, 266–276. https://doi.org/10.1016/j.epsl.2017.04.050

Taylor, K. C., Lamorey, G. W., Doyle, G. A., Alley, R. B., Grootes, P. M., Mayewski, P. A., White, J. W. C., & Barlow, L. K. (1993). The 'flickering switch' of late Pleistocene climate change. *Nature*, *361*(6411), Article 6411. https://doi.org/10.1038/361432a0

Teruggi, M. E. (1957). The nature and origin of Argentine loess. *Journal of Sedimentary Research*, *27*(3), 322–332. https://doi.org/10.1306/74D706DC-2B21-11D7-8648000102C1865D

Thomas, W. A., Astini, R. A., Mueller, P. A., Gehrels, G. E., & Wooden, J. L. (2004). Transfer of the Argentine Precordillera terrane from Laurentia: Constraints from detrital-zircon geochronology. *Geology*, *32*(11), 965–968. https://doi.org/10.1130/G20727.1

Toggweiler, J. R., Russell, J. L., & Carson, S. R. (2006). Midlatitude westerlies, atmospheric CO2, and climate change during the ice ages. *Paleoceanography*, *21*(2). https://doi.org/10.1029/2005PA001154

Tripaldi, A., Mehl, A., & Zárate, M. A. (2018). Parabolic megadunes in a subtropical Quaternary inland dune field, southwestern Pampas, Argentina. *Geomorphology*, *321*, 103–116. https://doi.org/10.1016/j.geomorph.2018.08.021

Tripaldi, A., & Zárate, M. A. (2016). A review of Late Quaternary inland dune systems of South America east of the Andes. *Quaternary International*, *410*, 96–110. https://doi.org/10.1016/j.quaint.2014.06.069

Tripaldi, A., Zárate, M. A., Forman, S. L., Badger, T., Doyle, M. E., & Ciccioli, P. (2013). Geological evidence for a drought episode in the western Pampas (Argentina, South America) during the early–mid 20th century. *The Holocene*, *23*(12), 1731–1746. https://doi.org/10.1177/0959683613505338

Vermeesch, P. (2021). Maximum depositional age estimation revisited. *Geoscience Frontiers*, *12*(2), 843–850. https://doi.org/10.1016/j.gsf.2020.08.008

Visconti, G., Melchor, R. N., Montalvo, C. I., Umazano, A. M., & De Elorriaga, E. E. (2010). Análisis litoestratigráfico de la Formación Cerro Azul (Mioceno Superior) en la provincia de La Pampa. *Revista de La Asociación Geológica Argentina*, *67*(2), 257–265.

Willner, A. P., Gerdes, A., & Massonne, H.-J. (2008). History of crustal growth and recycling at the Pacific convergent margin of South America at latitudes 29°–36° S revealed by a U–Pb and Lu–Hf isotope study of detrital zircon from late Paleozoic accretionary systems. *Chemical Geology*, *253*(3), 114–129. https://doi.org/10.1016/j.chemgeo.2008.04.016

Zarate, M. A., & Fasano, J. L. (1989). The Plio-Pleistocene record of the central eastern Pampas, Buenos Aires province, Argentina: The Chapadmalal case study. *Palaeogeography, Palaeoclimatology, Palaeoecology*, *72*, 27–52. https://doi.org/10.1016/0031-0182(89)90130-2

Zárate, M. A., & Tripaldi, A. (2012). The aeolian system of central Argentina. *Aeolian Research*, *3*(4), 401–417. https://doi.org/10.1016/j.aeolia.2011.08.002

Zarate, M., & Blasi, A. (1991). Late pleistocene and holocene loess deposits of the Southeastern Buenos Aires province, Argentina. *GeoJournal*, *24*(2), 211–220. https://doi.org/10.1007/BF00186018

Zárate, M., & Blasi, A. (1993). Late Pleistocene-Holocene eolian deposits of the southern Buenos Aires province, Argentina: A preliminary model. *Quaternary International*, *17*, 15–20. https://doi.org/10.1016/1040-6182(93)90075-Q

Zavala, C., & Freije, R. H. (2001). ON THE UNDERSTANDING OF AEOLIAN SEQUENCE STRATIGRAPHY: AN EXAMPLE FROM MIOCENE-PLIOCENE DEPOSITS IN PATAGONIA, ARGENTINA. *RIVISTA ITALIANA DI PALEONTOLOGIA E STRATIGRAFIA*, *107*(2), Article 2. https://doi.org/10.54103/2039-4942/16129

APPENDIX A

SAMPLE PROCESSING, FORMATION AGE CONSTRAINTS WITH REFERENCES, AND ANALYTICAL PROCEDURES

Standard sample processing techniques were used to separate zircons. A detailed description of the separation techniques are as follows:

1. Approximately 2.5 to 3 kg of sample was disaggregated using a mortar and pestle prior to sieving with a 1 mm sieve.
2. Grains were separated by density using a Gemini Shaking Table. The densest grains were then collected at the end of the Table for further processing.
3. Grains were dried and passed through a 500-micron sieve.
4. Grains were separated based on magnetic parameters using a hand magnet and Frantz Barrier Field Isodynamic Magnetic Separator. Samples were passed through the Frantz three times, first using a frequency of 0.3 amps, then 0.7 amps, and finally 1.0 amps. Non-magnetic grains after the 1.0 amps Frantz run were collected for further processing.
5. Samples were further processed by density using Lithium Metatungstate (2.95 g/cm^3). Grains denser than the heavy liquid sank to the bottom of the vile and were collected, cleaned using water, and bottled for transport to the University of Arizona for mounting and analysis.

Procedures for sample analysis were as follows:

1. The detrital zircon grains were mounted in resin pucks at the University of Arizona in preparation for analysis.
2. Zircon grains were analyzed at the University of Arizona LaserChron Center using a Nu-Plasma Multicollector Inductively-Coupled Plasma Mass Spectrometer (ICP-MS) using methods described in Gehrels et al, (2008).
3. Samples were analyzed with a laser spot size of 25 microns with the exception of 30 microns for samples AS1 and SI2.
4. Two reference materials, Sri Lanka and R33, were used to account for elemental and mass-fractionation instrument drift as well as down-pit fractionation (Paces and Miller, 1993; Black et al., 2004; Gehrels et al., 2008; Mattinson, 2010).
5. Data reduction and analytical corrections were made using an in-house Excel-based software called AgeCalc (Gehrels et al., 2006). Pb206/Pb207 ratios were used to date zircon grains that were less than 900 Ma post correction while Pb206/U238 ratios were used for zircon grains that dated greater than 900 Ma post correction. The rejection criteria are as follows: max 206/238 error of 10%, max 207/206 error of 10 %, max discordance of 20 %, max reverse discordance of 10 %.

Table A.1: Formation Age Constraints

Formation	Age (Ma)	Method and Citation
Santa Isabel	0.2 - 0.0	Mag Strat (Orgeira, 1990)
	unknown	SALMA Lujanian Zarate and Fasano (1989)
Arroyo Seco	unknown	SALMA Lujanian Zarate and Fasano (1989)
	0.78	Matuyama and Brunnes polarity boundary (Orgeira, 1990; Bidegain and Rico, 2012)
Miramar	0.78	Matuyama and Brunnes polarity boundary (Orgeira, 1990; Bidegain and Rico, 2012)
	1.78	Oluvai polarity boundary (Bidegain and Rico, 2012)
San Andres	1.78	Oluvai polarity boundary (Bidegain and Rico, 2012)
	2.6	SALMA and lower Matuyama polarity boundary (Cione and Tonni, 1995; Bidegain and Rico, 2012)
Vorohue	2.6	SALMA and lower Matuyama polarity boundary (Cione and Tonni, 1995; Bidegain and Rico, 2012)
	2.9	Appearance of Mustelidae, SALMA (Cione and Tonni, 1995)
Barranca de los Lobos	2.9	Appearance of Mustelidae, SALMA (Cione and Tonni, 1995)
	3.04	Appearance of Camelidae (Cionne and Tonni, 1995)
Chapadmalal	3.04	Appearance of Camelidae (Cionne and Tonni, 1995)
	3.74	40AR/39Ar dating of escoria in Lower and Upper Chapadmalal (Prevosti et al., 2021)

APPENDIX B

SUPPLEMENTARY FIGURES

The figures present within Appendix B were created using Multidimensional Scaling (MDS). MDS works by measuring dissimilarities between samples, therefore, samples that plot close to one another contain fewer dissimilarities than samples that plot far from one another.

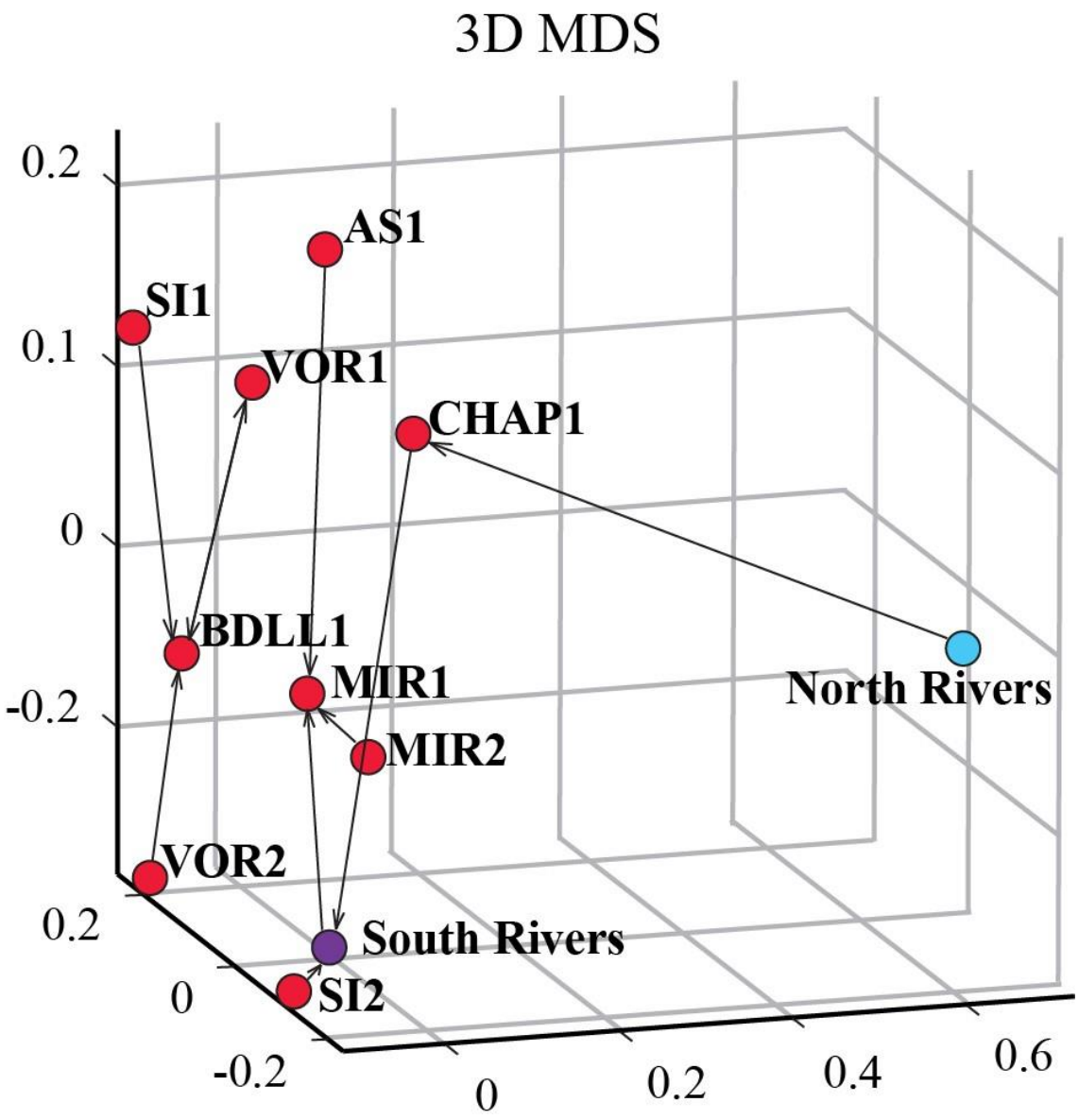

Figure B.1: MDS Figure showing the similarities between my samples (red) and the rivers present in the southern latitudes (purple).

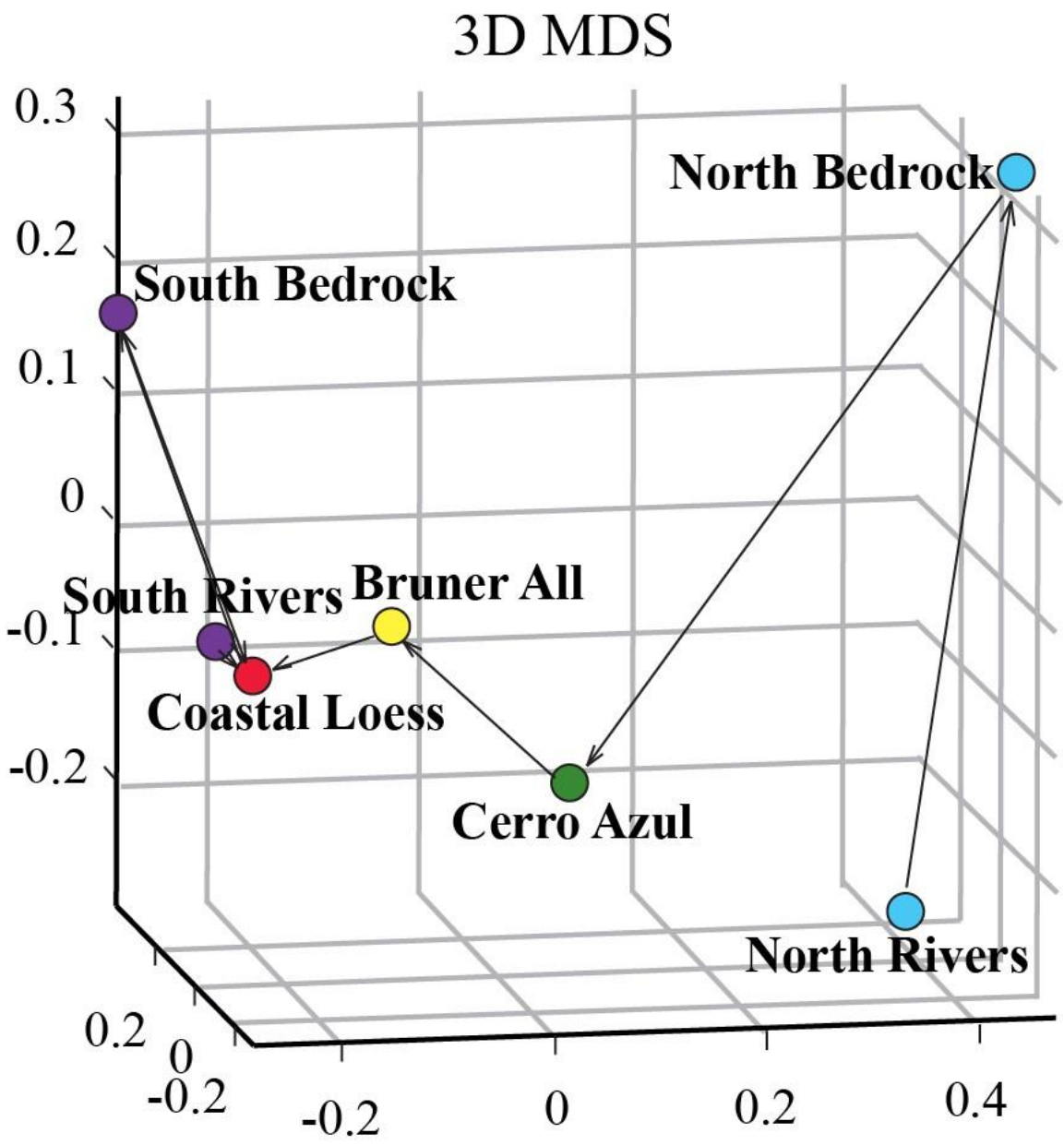

Figure B.2: MDS showing my samples (red) with respect to the Late Pleistocene/Holocene samples found in Bruner et al., (2022) (yellow), the Cerro Azul samples found in Stubbins et al., (2023) (green), the north zone data (blue), and the south zone data (purple).

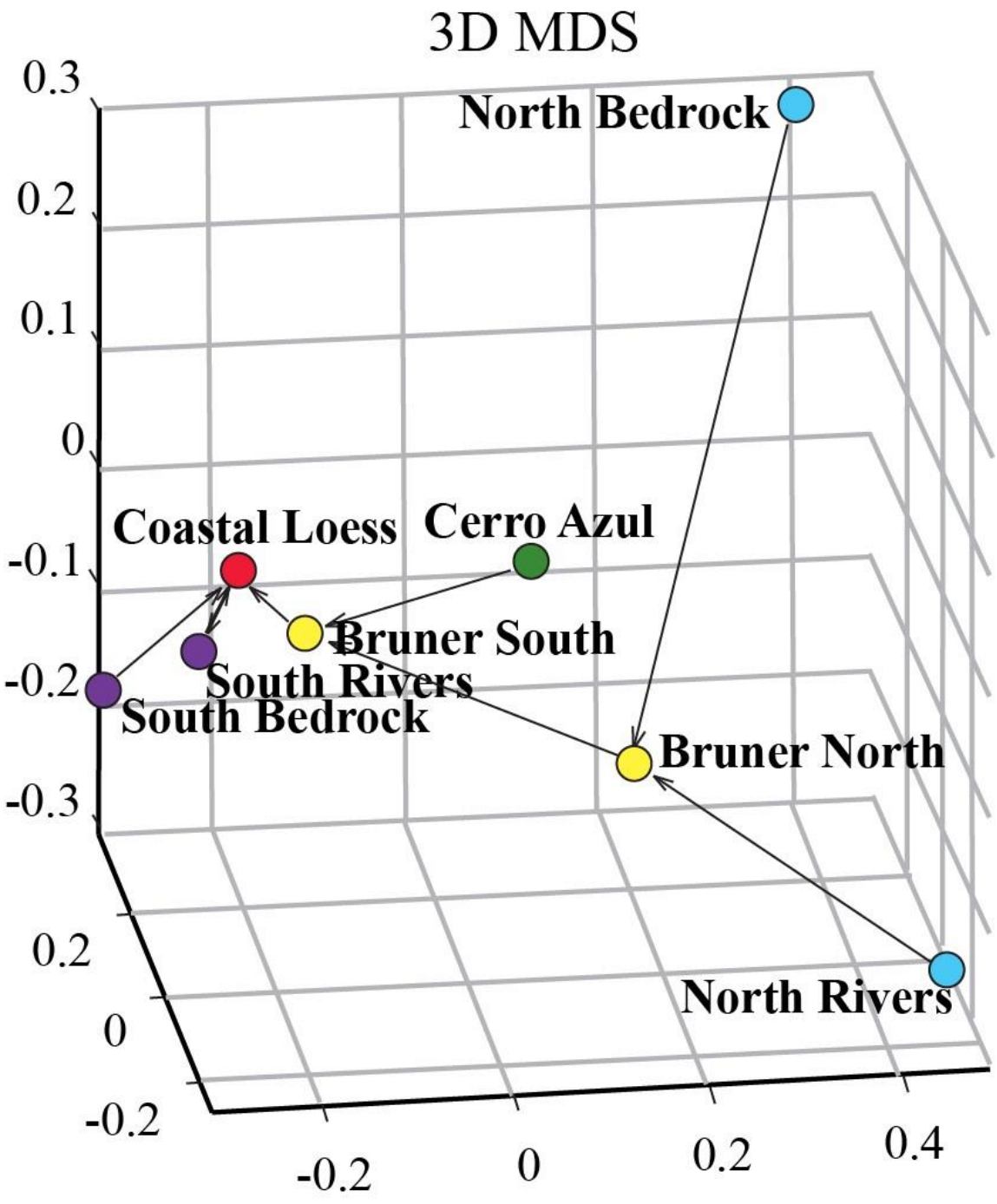

Figure B.3: Same as Figure B.2 but the Late Pleistocene/Holocene data from Bruner et al., (2022) has been split between the same 35° S latitude lines as the source zones.

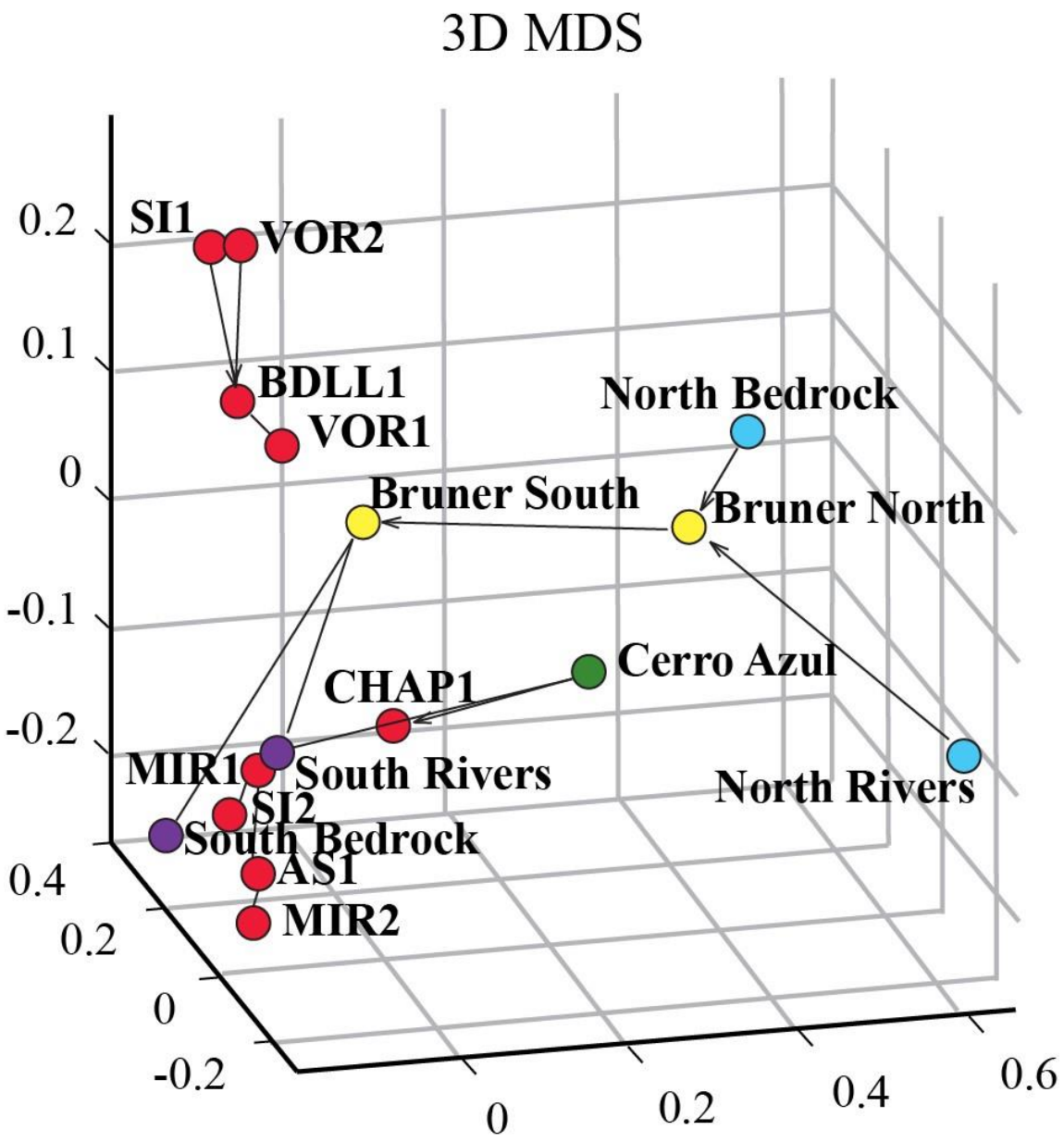

Figure B.4: Same as Figure B.3 but my samples have not been combined into one data point.

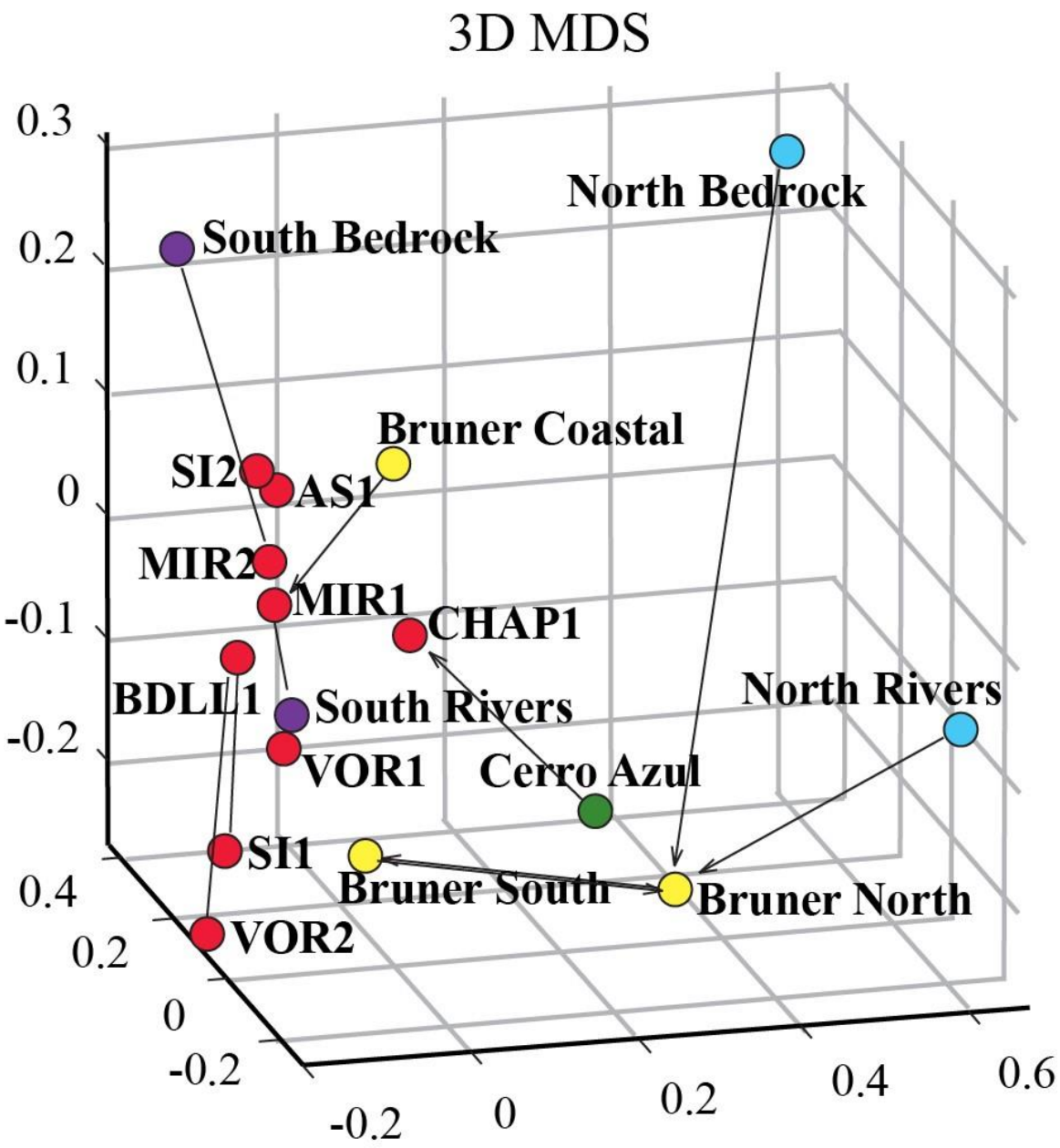

Figure B.5: Same as Figure B.4 but the two coastal samples from the Bruner South dataset have been separated out and put in as Bruner Coastal.

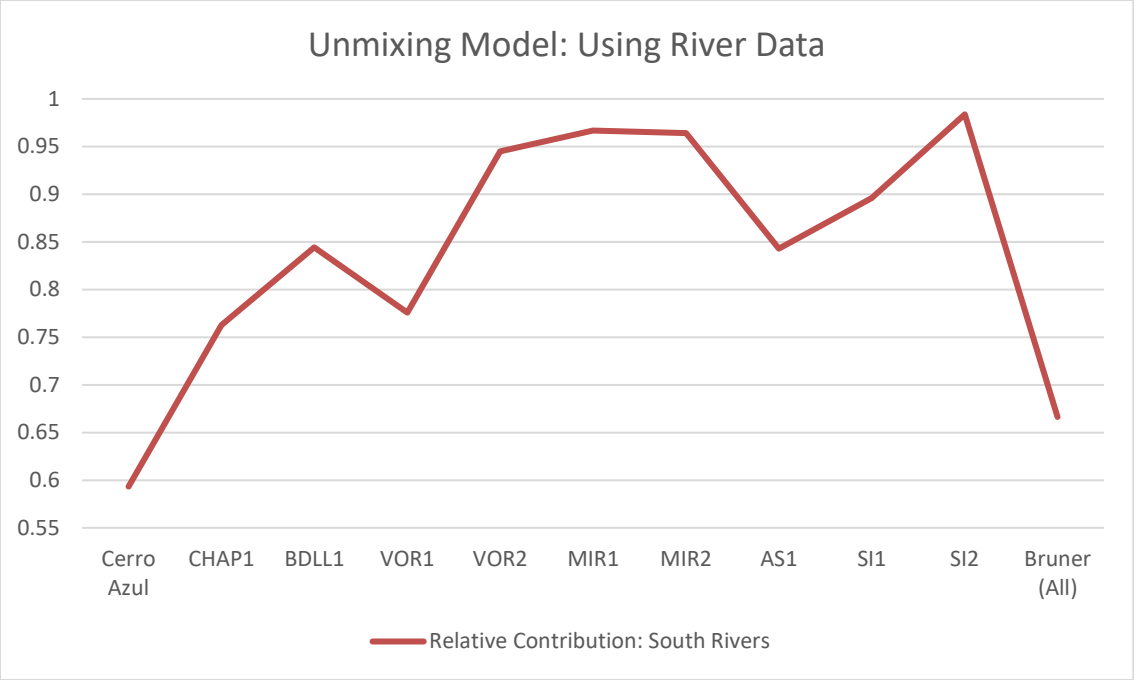

Figure B.6: Unmixing model results for my samples with the inclusion of samples from the Cerro Azul and all combined samples from Bruner et al., (2023). The y-axis shows contribution of the southern rivers for each sample.